RECOMBINANT ADENO-ASSOCIATED VIRUS AS A THERAPEUTIC THERAPY FOR PLN R14DEL PATIENTS

Thesis of Sam Biermans
07-01-2021
Supervisor: Dr. Niels Bovenschen
Second assessor: Dr. Cathy Moelans

Table of content

Graphical abstract

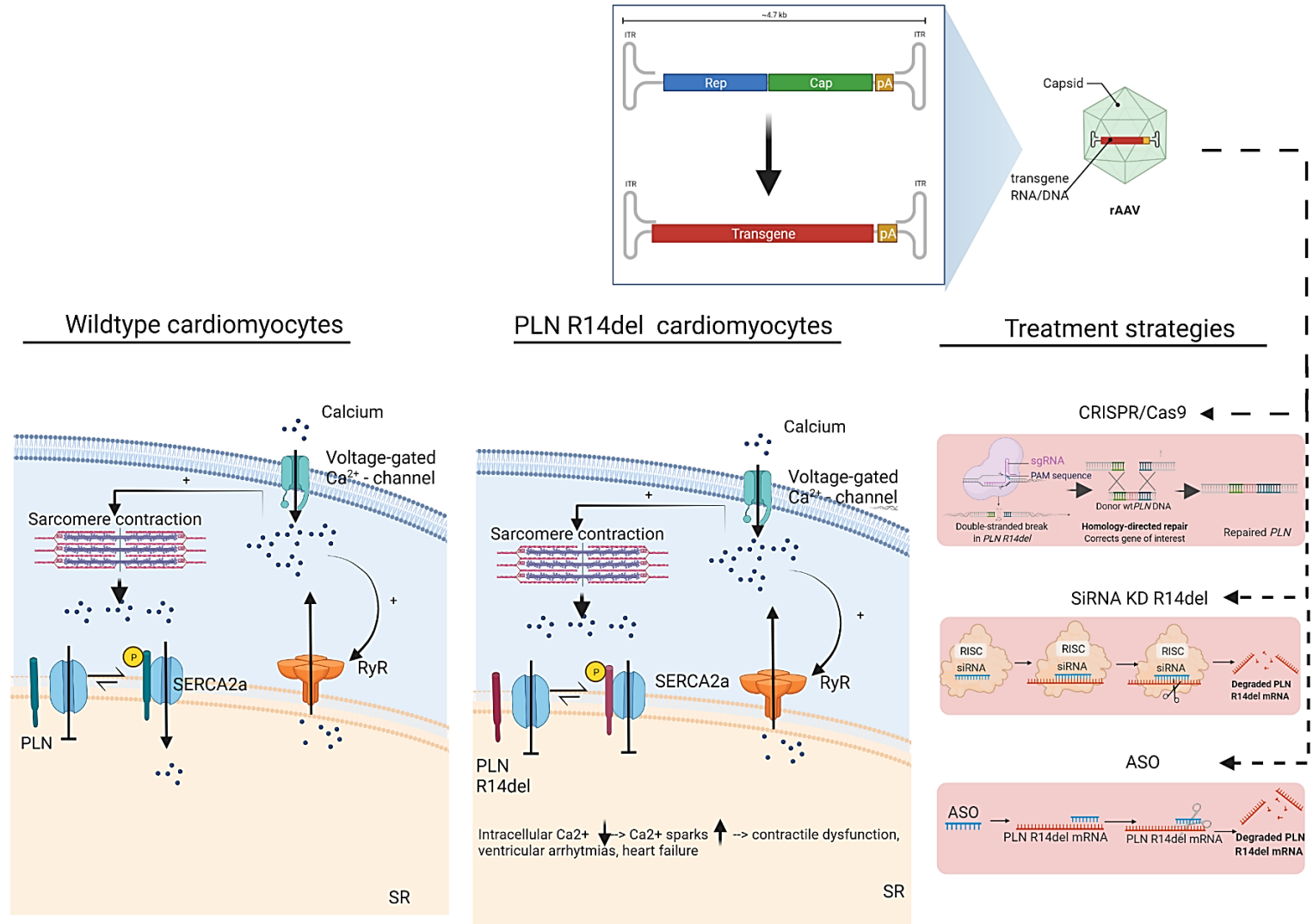

Abstract

Gene therapy has gained significant momentum over the past few years and recombinant adeno-associated viruses (rAAVs) have developed to be the leading platform for *in vivo* gene therapy delivery. These rAAVs are capable of transducing a broad spectrum of proliferating and quiescent cell types, long-term transgene expression upon once-off delivery, and have low immunogenicity. One field that is in desperate need for new therapeutics, is heart failure (HF). HF remains a significant health burden and leading cause of death, with little available treatments that focus on delaying disease progression and managing symptoms, rather than curing. For a specific subgroup of HF patients, caused by an underlying deleterious mutation p.(Arg14del) in the phospholamban (PLN) gene, treatment is completely lacking. Currently, efforts to develop tailored therapies for these patients are ongoing, using rAAVs as gene delivery vehicles. These vectors are modified to encapsulate and deliver state of the art technologies such as; clustered regularly interspaced short palindromic repeats and CRISPR associated protein 9 (CRISPR-Cas9) to correct the mutated *PLN* gene, short interference RNAs (siRNAs) and antisense oligonucleotides (ASOs) to inhibit PLN R14del mRNA translation and thus the production of the mutated protein. In order to create viable AAV-therapeutics, additional developments in understanding the AAV biology, in trials, and in long-term clinical experience is needed. This will guide the generation of rAAVs which are modified to become non-immunogenic, more specific, and efficient by interfering with the AAV transgenic genome, capsid, and steps in the AAV life cycle. Although more advances have to be made, the way towards a cure for PLN R14del patients is slowly paved. With the development in finding therapeutics for this specific cardiovascular disease, bridges will be built towards the utility of these strategies for a plethora of other diseases.

List of abbreviations

HF: *heart failure*
AAV: *adeno-associated virus*
PLN: *phospholamban*
DWORF: *Dwarf Open Reading Frame*
R14del: *Deleterious mutation of the arginine 14 codon in the PLN gene*
mRNA: *messenger RNA*
CRISPR-Cas9: *clustered regularly interspaced short palindromic repeats and CRISPR associated protein 9*
RMK: *rhesus-monkey-kidney*
SV15: *simian adenovirus type 15*
CPE: *cytopathic effect*
ORF: *open-reading frame*
VP: *viral capsid protein*
aa: *amino acid*
VP1u: *VP1 unique region*
PLA2: *phospholipase A2 enzyme*
NLS: *nuclear localisation signal*
βA: *β-strand A*
αA: *conserved α-helix*
VR: *variable region*
Bp: *basepairs*
Rep: *AAV replication gene giving rise to Rep proteins*
Cap: *AAV capsid gene encoding VP1, VP2, and VP3*
MAAP: *membrane-associated accessory protein*
AAP: *assembly activating protein*
ITR: *Inverted terminal repeat*
RBE: *Rep binding element*
trs: *terminal resolution site*
HSPG: *heparan sulphate proteoglycan*
CLIC/GEEC: *carriers and GPI-anchored-protein-enriched early endosomal compartment*
ARF1: *ADP-ribosylation factor 1*
Cdc42: *cell division control protein 42 homolog*
TGN: *Trans Golgi Network*
STX5: *syntaxin 5*
NPC: *nuclear pore complex*
NPM: *nucleophosmin*
Ss: *single-stranded*
Ds: *double-stranded*
scAAV: *self-complementary AAV genome*
hAdV5: *adenovirus type 5*
rAAV: *recombinant adeno-associated virus*
AdV: *adenovirus*
HSV: *herpes simplex virus*
BV: *baculovirus*
HEK: *human embryonic kidney*
Vp/cell: *viral production per cell*

BHK: *baby hamster kidney*
Sf9: *Spodoptera frugiperda 9*
DCM: *Dilated cardiomyopathy*
SR: *Sarcoplasmic reticulum*
RyRs: *Ryanodine receptors*
SERCA**:** *sarco(endo)plasmic reticulum* Ca^{2+}*-ATPase*
PKA: *protein kinase A*
hiPSC-CMs*: human induced pluripotent stem cell-derived cardiomyocytes*
ZFNs: *Zinc finger nucleases*
TALEN: *transcription activator-like effector nucleases*
miR-PLN: *intronic artificial microRNA against PLN*
HCM: *hypertrophic cardiomyopathy*
HDR: *homology-directed repair*
RISC: *RNA-induced silencing complex*
LNA: *locked nucleic acids*
ASO: *antisense oligonucleotides*
MLP: *muscle-specific LIM domain protein*
KO: *knock-out*
hECT: *human engineered cardiac tissues*
WB: *Western Blot*

Introduction

The world is currently trying to get back on its feet, after severe acute respiratory coronavirus 2 whiplashed the entire world with over 180 million reported cases and 4 million deaths at the time of writing[1]. This pandemic has led to normalisation of wearing face masks, social distancing, international travel-related control measures, and to total lockdowns that took away all freedom. This generated enormous awareness of the impact of viruses on human society and made it almost impossible to believe that these parasites could also be used to cure diseases and function as a tool for research. However, some viruses can be modified to deliver therapeutic genes to cells in order to cure or treat patients instead of causing disease, for instance to treat heart failure[2].

Heart failure (HF) remains a significant public health burden and a leading cause of death, with little available treatments that mainly focus on delaying disease progression and managing symptoms[3,4]. In recent years, advances in treatment have been made and gene therapy has arisen as a promising platform for the treatment of HF[5]. Adeno-associated virus (AAV) vectors have become the most widely used gene delivery vehicle and they have yielded highly promising results, due to their safety in the clinic, broad tissue tropism, and long-term transgene expression[6,7]. The potential of these vectors for cardiac gene therapy has also been recognised and this has led to the evolution of AAV vectors efficient at gene delivery to the heart[8]. AAVs have been optimised by novel capsid discovery and engineering, promotor optimisation, and by developing immune-evasion strategies[8].

Currently, a proven effective treatment for HF patients, suffering from a specific pathogenic mutation, is still lacking. This deleterious mutation, named phospholamban (PLN) R14del, is associated with prevalent ventricular arrhythmias, contractile dysfunction, HF, and sudden cardiac death[9,10]. Gene therapy using AAV vectors might be a promising novel strategy to tackle this disease[11]. Therefore, the following research question arose: “How can adeno-associated viruses be transformed into a gene delivery vehicle and be used for new therapeutic treatments for PLN R14del patients?”. In order to answer this question, several topics need to be addressed. In Chapter 1, the origin of virology, the basic concepts of viruses, and the shift towards a virus’ therapeutic potential is explained. Chapter 2 and 3 provide insight into the biology of AAV and its normal life cycle, necessary to understand the adaptations needed to produce gene delivery vehicles from AAVs (Chapter 4). Moreover, this thorough description of the viral life cycle sheds light on rate-limiting steps of transduction and on features that need to be considered to generate specific and effective vectors. Furthermore, Chapter 4 describes the PLN R14del phenotype, the mechanisms of disease, and three ongoing therapeutic research, using recombinant AAVs as a gene therapy approach.

Interestingly, a recently identified micro peptide named Dwarf Open Reading Frame (DWORF) is discussed in Chapter 5, which has potential in reversing the PLN R14del phenotype[12]. In order to prove its effect on PLN R14del mutations, an experiment has been performed that will provide mechanistic understanding of how DWORF could neutralise PLN R14del-induced super-inhibition. This information could lead to a promising lead to develop a novel targeted therapy for PLN R14del patients.

Therefore, the aim of this literature review and cutting edge research is to provide a thorough understanding of AAVs and their use for gene therapy, specifically for PLN R14del. The light shed on current investigations will highlight the potential of AAVs to find a treatment for these patients and the outcome of the experiments will hopefully open doors for the application of this technique for many other (HF) illnesses.

Chapter 1: Intracellular obligate parasites

Written history indicates that viruses arose as disease-inciting agents about 600 years or more ago, but theory suggests that these parasites may be as old as life itself[13,14]. However, the science of viruses dates back to barely 130 years ago[14]. At that time, it was unimaginable that this entity would turn out to be a tool for research and therapeutic strategies, so viruses were named after the Latin word *virus,* meaning poison[2].

1.1 The discovery of viruses

Viruses were first described in the closing years of the 19th century[15,16]. Until that time, people were aware of many human and animal diseases, but the concept of a virus as a distinct entity was undiscovered[15]. However, at that moment, ideas such as vitalism and belief in spontaneous generation, began to lose ground and subjects like agricultural chemistry and microbiology started to emerge as new disciplines[16]. Bacteriology and Koch's postulates began to dominate the study of disease and the postulates were even converted into a *dogma* that stated: 'tout virus est un microbe' (viruses are always microbes)[16,17]. At the end of this century, a change of heart was made about this subject, thanks to the devotion of three botanical scientists[2,15,16,18,19].

In 1879, a German agricultural chemist named Adolf Eduard Mayer was requested to research a disease of tobacco plants that had plagued local farmers in the Netherlands. Diseased leaves of this plant showed heterogeneously pigmented spots and the affliction was named 'tobacco mosaic disease'[2]. At that time, microbes were thought to underlie many diseases, so Mayer performed microbiologic experiments to prove a microbial aetiology[2,18]. He discovered that inoculation of healthy plants with sap expressed from leaves of diseased plants, let to transmission of the disorder[2]. However, when transferring the sap of the diseased plants through laboratory filters, the agent remains infectious[18]. This was unlike bacteria, which were too large to pass through these bacterium filters. Mayer still assumed that the pathogen was of a bacterial origin, but he suggested its similarity to enzymes and he named this novel aetiologic agent a 'soluble, possibly enzyme-like contagium'[2,15,18,19].

Mayer shared his findings with Martinus Beijerinck, a chemist with interests in botany[2]. Beijerinck reviewed Mayer's experimental data and he performed additional experiments, which resulted again in an inability to demonstrate the presence of microbes[2]. Nonetheless, he admitted that this could be attributed to his incomplete bacteriological knowledge at that time[16]. The academic phase of Beijerinck's career began in 1895, when he was appointed Professor of Bacteriology at the Polytechnical school at Delft[16]. He decided to resume the study of the tobacco mosaic disease and he published the following three conclusions in 1899: (I) The tobacco mosaic infection is not caused by microbes, but by a non-corpsular (non-cellular) entity, which he named *'contagium vivum fluidum'*. (II) The virus multiplies only in growing plant organs where cellular division takes place. (III) The virus is inactivated by boiling, but can be dried without losing its infectious properties[16,19,20]. Hereby, a new subcategory was defined within all sorts of venomous agents; the filterable viruses.

The year after Beijerinck's first reports, the Russian scientist Dmitri Iosifovich Ivanovsky reported that he had priority in discovering the filterable nature of the tobacco mosaic disease[2,18,19]. He had discovered this as early as 1892 and this was acknowledged by Beijerinck, who additionally stated that he was unaware of Ivanovsky's investigations. Like Beijerinck and Mayer, Ivanovsky too demonstrated the filterable nature of this disease and the infectiousness of the filtrate[2,18,19]. However, he had denounced Mayer's conclusion about the loss of infectivity of the filtrate after passage through the Chamberland filters[2]. He reported that the sap of leaves attacked by the mosaic disease retained its

infectious qualities, even after filtration. This was indeed a landmark in the history of virology, but as with Mayer, he interpreted his findings in the context of bacterial aetiology and assumed that his results represented the presence of other filterable materials such as bacterial toxins[2,18,19].

All three of them are seen as the founding fathers of virology and their findings unleashed a torrent of scientific investigations that revolutionised medicine and ushered the golden age of vaccinology[2,15,16,20]. By the end of the first quarter of the 20th century, over 65 diseases of animals and humans were found that could be attributed to these filterable agents; viruses[2,15,16,20].

1.2 Characterisation of a virus

After the discovery of this infectious entity, information on viruses has been growing exponentially. Developments in the field of molecular biology and virology went hand-in-hand with growth of experimental and computational techniques[21]. Information about size, shape, and properties of viruses became known when Wendell M. Stanley succeeded in isolating the tobacco mosaic virus from diseased leaves in 1935[22]. Analysis with a polarising light microscope indicated the presence of a well-ordered substance, and this phenomenon was further exploited by Bernal and Fankuchen in 1941[23]. With the use of X-ray diffraction, the first detailed description of a virus structure was generated[21,23]. The virus structure was further clarified by many scientists, over many years, using techniques such as X-ray crystallography, (cryo-)electron microscopy, and tomography[21,23]. This has led to great insights into the structure and lifecycle of viruses.

The definition of a virus, however, cannot be described in one sentence or in a single paragraph, as viral diversity is far greater than that of any other organism[24–27]. Nowadays, viruses are defined as small infectious agents with an acellular organisation, that depend on the synthesis machinery of susceptible living cells to get reproduced[27]. Viruses are classified based on three factors; genome organisation, morphology, and mode of replication[24]. Viruses contain, by definition, either a DNA or RNA genome that is surrounded by a protective, virus-coded protein coat (Figure 1)[24–27] . This protein coat consists of at least 60 proteins with structural properties that permit regular and repetitive interactions among them[24–27]. Some viruses additionally contain a host cell-derived lipid bilayer that contains viral glycoproteins that cover the protein coat. This layer is called the viral envelope. Their viral genome may be single- or double-stranded, can be circular or linear, and it may occupy one nucleic acid molecule, or segmented molecules[24,27]. These segments can subsequently be packaged together, or can be distributed over separate virus particles[27]. Moreover, the size of viral genomes ranges from less than 2,000 bases, containing only two genes, to 2.5 million base pairs, containing over 2,500 genes[27,28]. This variation reflects not only the diversity of replication mechanisms and cellular interactions, but it also shows the variation in structural complexity of their transmission vehicle, called a virion[27]. A virion is the extracellular appearance of a virus particle that makes the virus infectious. It enables the genome to be delivered into the host cell, so that it can be expressed[24,25]. Moreover, the virion condensates and packages the genome and protects it within and outside the organism[24,25].

A prerequisite of viral replication is expression of the viral genome for the production of (non-) structural viral proteins that aid in the viral life cycle[24]. Therefore, messenger RNA (mRNA) must be produced in the host cell. How viruses produce *de novo* mRNA from their genome, is referred to as the Baltimore classification and this mode of replication attributes to the classification of viruses[24]. The viral genomes can be broken down into seven groups that use different replication strategies[24]. These strategies depend on the incoming DNA/RNA genome, being single-stranded, double-stranded, positive or negative, and the virus itself[24]. A positive-strand genome can function as mRNA and can be directly transcribed within a host cell, giving rise to viral proteins. However, this is not *de novo* mRNA

and replication of the genome has to occur first to give rise to *de novo* positive-strand genomes. A negative-strand genome cannot be expressed before it is transformed into a positive-strand, immediately producing *de novo* mRNA. Moreover, some viruses even use a reverse transcriptase enzyme to create a DNA genome from a RNA genome, which can then function as a mRNA template[24]. These examples highlight the many different replication strategies that are used by viruses and that are used for viral classification.

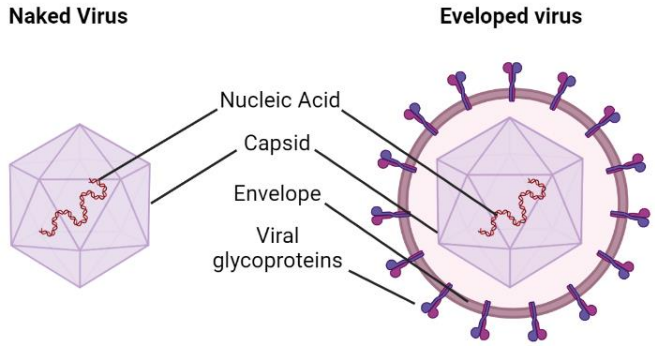

Figure 1: Schematic representation of a virus structure. *The nucleic acid of naked viruses is protected by a virus-coded protein coat. Enveloped viruses additionally contain a host cell-derived lipid bilayer that covers the protein coat. This bilayer contains viral glycoproteins. Created with BioRender.*

1.3 Viruses and their therapeutic potential

The emergence of virology has been fundamental to increase our understanding of several subjects, ranging from basic characteristics of cell biology to the most advanced biochemical processes[26]. From the 20th century and onwards, research on viruses has increased tremendously. Up until then, viruses were seen as pathogens that were only harmful, but research into the discipline of virology actually formed the basis of great discoveries that have revolutionised the field of medicine and biotechnology[26,29].

In particular, studies on DNA viruses have been one of the most important sources that have led to the development of a novel group of biotechnological tools[29]. These DNA-based therapeutics include viral therapies against bacterial infections, use of restriction enzymes for molecular cloning, clustered regularly interspaced short palindromic repeats and CRISPR associated protein 9 (CRISPR-Cas9) system for precision gene editing, and plasmids that contain transgenes for gene therapy[29–31]. The latter two biotechnological tools are discussed further in Chapter 4. These techniques are evolving into viable strategies for the development of therapeutics for a wide range of human disorders, including cancer, AIDS, neurological disorders, and cardiovascular diseases[29–31].

More specifically, the use of AAV for therapeutic and investigational tools has gained significant momentum over the past two decades[32]. The AAV was originally discovered in the mid-1960s as a contaminant of a cell culture that was also infected with an adenovirus[32–35]. AAV is a small virus that is an ubiquitous commensal for humans that is classified in group 2 of the Baltimore classification (Figure 2). Interests in the AAV molecular biology started to arise in the mid-1980s, fostered by the discovery that DNA viruses might be used as gene delivery vectors[32–34]. In 1984, a seminal study by Hermonat *et al*. was the first to demonstrate the utility of AAV as a mammalian gene transfer vector[36]. Since then, numerous pre-clinical and clinical studies have been conducted and AAV vectors are now widely used for their therapeutic potential as well as their outstanding investigational options[36]. AAV vectors have a high efficiency of transduction of both non-dividing and dividing cells, drive of efficient and persistent transgene expression, and an expanded tropism[32–34]. The biology of AAVs is discussed in Chapters two

and three, and Chapter four elaborates on the development and use of these vectors for cardiac gene therapy.

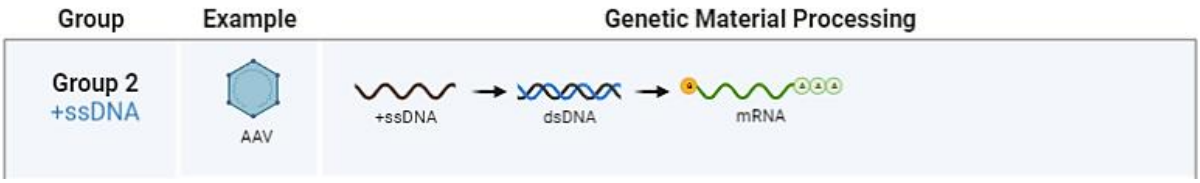

Figure 2: The Baltimore classification of AAV. *The AAV contains a ssDNA genome. In order for the virus to replicate, the genome is converted to a dsDNA genome using synthesis machinery from the host cell. From this dsDNA genome, de novo mRNA can be created. mRNA is used for translation of viral genes. dsDNA, double-stranded DNA; mRNA, messenger RNA; ssDNA, single-stranded DNA. Created with BioRender.*

Chapter 2: The biology of adeno-associated viruses

Adeno-associated viruses are among the smallest members of the animal viruses with DNA genomes[37]. Their genome has a unique structure and new insights are still gained of its coding capacity. The AAV capsid is seen as the most simple icosahedral structure, but variations within its coding sequence led to the origin of many AAV serotypes[37].

2.1 Discovery and classification of adeno-associated virus

The AAV virus was first discovered in 1965 in a pooled harvest of rhesus-monkey-kidney (RMK) cell cultures, which were infected with the simian adenovirus type 15 (SV15)[34]. These cells showed complete cytopathic effects and were lysed, centrifuged, and purified until merely virus particles were left[33,34]. Electron microscopy revealed that SV15 preparations contained high concentrations of unknown small, uniform, virus-like particles, together with SV15 particles[33,34]. The virus-like particles were separated from the SV15 particles and RMK cultures were inoculated with the suspension. Strangely, no cytopathic effect (CPE) occurred in cell cultures that were only infected with the virus-like particles. On the contrary, CPE was seen when the suspension of virus-like particles was added to cell cultures co-infected with SV15[33,34]. This gave rise to the phenomenon that these particles need the presence of a helper virus for successful replication, and it was named adeno-associated virus[33–35,38].

The adeno-associated virus belongs to the *Parvoviridae* family and the *Parvovirinae* subfamily[39–41]. This subfamily is characterised by a genome that contains several open reading frames (ORF), of which one encodes a series of regulatory proteins with a highly conserved SF3 helicase domain. The conservation of this domain is used for the classification of the parvoviruses into different genera[40]. Moreover, the phylogeny of this domain additionally corresponds to the host range of different subfamilies and the hosts of the *Parvovirinae* can therefore only be found in vertebrates[39–41]. The subfamily is divided into 10 genera, of which AAV is categorised within the genus *Dependoparvovirus*[38]. This genus contains viruses with an inability to replicate productively in a host cell, without the presence of a helper virus, such as an adenovirus, a herpesvirus, or a vaccinia virus[35,38]. The helper adenovirus produces early genes E1A, E1B, E4, and E2A, which induce S-phase in the host cell and provide components needed for successful viral DNA expression, replication, and transduction (see Chapter 3)[35,38,42].

Unlike most viruses, AAVs are innately non-pathogenic, poorly immunogenic, and they have a broad tropism[43]. They are capable of infecting many cell types from humans and some other primate species, but they have never been linked to illnesses[43]. The efficiency of their infection is dependent on the AAV serotype[33,35]. There are over 100 AAV genomic isolates and 13 serotypes described since 1965, of which AAV2 is studied the most[44]. These serotypes have a similar structure, genome size, and

organisation, but differ in their tropism and types of cells they infect, dictated by their capsid sequence [33,35,43]. The serotypes are discussed further in Chapter 2.4.

2.2 AAV capsid structure

AAV viruses are one of the smallest virus classes, containing a non-enveloped icosahedral capsid of approximately 25nm[38,40,41]. The capsid is composed of 60 viral structural subunits, each consisting of three types of structural proteins (VP1, VP2, and VP3). These subunits are organised in T=1 icosahedral symmetry, via 2-, 3-, and 5-fold symmetry-related interactions[40,45,46]. This means that the structural subunits are in a structurally identical environment and display equivalent interactions with their neighbours[40,45,46]. The major capsid component, VP3, is a 59-61-kDa protein that constitutes 90% of the capsid's protein content. The sequence of this VP is referred to as the VP3 common region, as it is shared among all VPs. However, the other two VPs show extended N-termini and have different molecular masses[47,48]. The VP2 protein is 57 amino acids (aa) longer than VP3 and has a molecular weight between 64-67 kDa. The N-terminus of this VP is referred to as the VP1/VP2 common region. VP1, on the other hand, is 137 aa longer than VP2 and has a molecular weight between 79-82 kDa. This region is called the VP1 unique (VP1u) region and it contains an essential phospholipase A2 (PLA2) enzyme[48]. Moreover, the VP1u and the VP1/VP2 common region contain nuclear localisation sequences (NLSs) and their N-terminal extensions are crucial for endosomal trafficking and escape, nuclear localisation, and genome release (Chapter 3)[48].

Determination of the AAV capsid structure, revealed the VP monomers to all display similar structures (Figure 3A)[48,49]. The VP structure consists of a conserved eight stranded anti-parallel β-core (designated βB- βI), also known as a jelly roll motif, with a BIDG sheet that forms the inner surface of the capsid[40,46]. Additionally, a β-strand A (βA), which runs anti-parallel to the βB strand of the BIDG sheet, and a conserved α-helix (αA) located between strands βC and βD, are also part of the conserved core structure[40,46]. Together, they form the contiguous capsid shell, while large inter-strand loops form the majority of the capsid surface. These loops are formed out of small stretches of helical and β-strand structures and they are named after the β-strands they connect. Moreover, the apexes of the loops are named variable regions (VRs). The variety within these loops leads to distinct capsid morphologies, giving rise to different AAV serotypes[48,49].

However, the capsids still share the same overall characteristic features (Figure 3B)[40]. A conserved cylindrical channel is located at the icosahedral 5-fold axis, which is formed by five radial β-ribbons. These ribbons consist of two small stretches of β-strand structures that connect the βD and βE strands. The channel connects the interior of the capsid to the exterior and plays an important role in endosomal escape and genome packaging (Chapter 3)[40,46]. The channel itself is surrounded by a depression, formed by a structurally conserved loop between βH and βI (HI loop)[40,46]. Moreover, protrusions are found, formed from intertwining loops of VP3 monomers, that surround the 3-fold axes. Lastly, depressions are located at the 2-fold symmetry axes of the capsid. The walls of this depression are formed by conserved α-helices and they surround the 5-fold axis. The 2/5-fold walls serve as receptor-binding sites as well as anti-body binding sites[40].

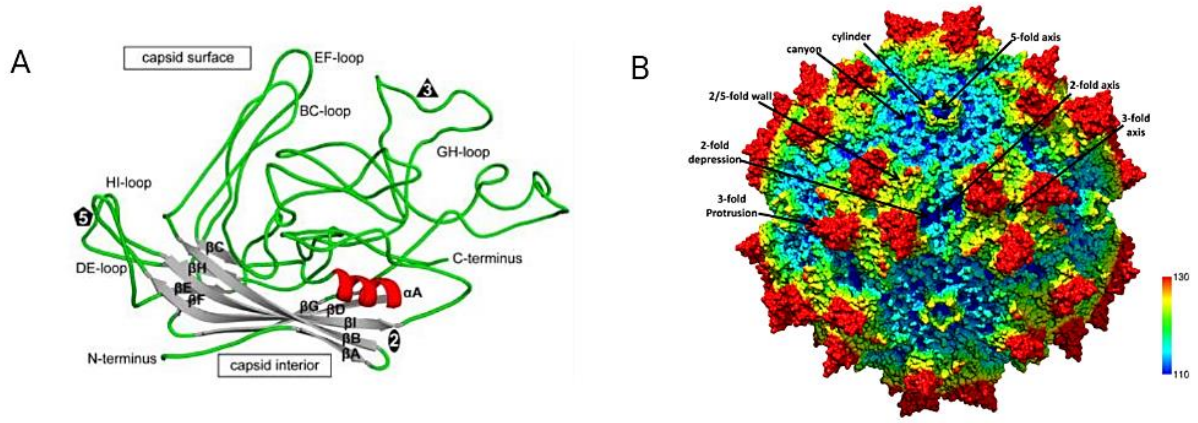

Figure 3: Capsid structure of an AAV virus. *(A) Cartoon ribbon diagram of an AAV VP monomer structure. Visual representation of the strands lining the capsid interior and capsid surface. The beta strands are depicted in grey (βA-βI) and the αA in red. The interconnecting surface loops and the N- and C-terminus are indicated in green. The approximate icosahedral 2-, 3-, and 5-fold axes are indicated via an oval, triangle, and pentagon. Adapted from Mietzch et al. (2019). (B) The AAV capsid is generated from 60 VP monomers. The characteristics of the capsid are shown and indicated by arrows and labelling, as well as the icosahedral 2-, 3-, and 5-fold symmetry axes. From capsid to surface: blue-green-yellow-red. Adapted from Tseng et al. (2014). αA, α-helix; AAV, adeno-associated virus; VP, viral capsid protein.*

2.3 AAV genome

The AAV carries a linear single-stranded DNA genome that ranges in size from 4642 base pairs (bp) to 4767 bp, dependent on the AAV serotype[35,38,50]. In 1982, the genome configuration and composition of the AAV2 serotype was the first to be clarified[38]. It was found that the AAV2 genome consists of both antisense and sense DNA strands, which are packaged separately into AAV capsids with equal frequency[38]. The AAV2 genome encodes ORFs for two viral genes, the *rep* (replication) gene and the *cap* (capsid) gene (Figure 4A). The *rep* gene encodes sequences for a series of regulatory proteins and the *cap* gene for the production of three viral capsid proteins and two additional proteins[35,38,51].

Multiple proteins can be formed out of the *rep* gene, through the use of two promotors, p5 and p19, and an internal splice donor and acceptor site (Figure 4A)[35,38,51]. Through this mechanism, the *rep* gene is capable of encoding four regulatory proteins that are respectively named Rep78, Rep68, Rep52, and Rep40[35,38,41]. The Rep78 and Rep68 proteins are produced from unspliced and spliced transcripts, using the p5 promotor, and function as important regulatory proteins that act in *trans* in all phases of the AAV life cycle[35,38]. This means that the regulatory proteins modify or regulate the expression of genes that are not located on the same strand but lie further away, whereas regulation of the activity of adjacent DNA sequences is referred to as acting in *cis*[52]. The Rep52 and Rep40 proteins are created using unspliced and spliced transcripts from the p19 promotor. These two proteins are involved in accumulation of single-stranded viral DNA molecules which are packaged inside AAV capsids (Chapter 3)[35,38]. All four regulatory proteins contain helicase and ATPase activity and Rep78 and Rep68 proteins additionally possess strand- and site-specific endonuclease and DNA binding activity[35,38,41].

On the other hand, the *cap* gene is transcribed using a single promotor, namely p40 (Figure 4A)[38]. This gene encodes five ORFs and uses alternative splicing and overprinting processes for the generation of three viral capsid proteins and two additional proteins[53–55]. However, until recently, the *cap* gene was believed to only produce two transcripts that encode three viral capsid proteins. The biggest capsid protein, VP1, was believed to be generated from the unspliced transcript and the spliced transcript was thought to only give rise to VP2 and VP3. These two proteins were separately created, using a nonconventional ACG start codon for the translation of VP2 and a downstream conventional AUG codon for VP3[35,38,41]. Rather, the unspliced transcript does not only generate the VP1 capsid protein, it

does also lead to the production of a newly discovered protein called membrane-associated accessory protein (MAAP)[53,55]. The *cap* gene contains a nonconventional CTG start codon, leading to production of this protein that is associated with the cell membrane[53,55]. Moreover, it was discovered by Sonntag *et al.* (2010) that a third gene is encoded within the *cap* coding sequence, that also uses a different reading frame[54–56]. This gene leads to production of assembly activating protein (AAP) that stimulates the transport of unassembled VP proteins into the nucleus for capsid assembly (Chapter 3)[54–56].

These overlapping gene arrangements are thought to originate by a process called overprinting[53,55]. Due to mutations in an ancestral reading frame, expression of a second reading frame is enabled, while the expression of the first frame remains preserved[53,55]. As a consequence, each pair of overlapping frames consists of one ancestral frame and one *de novo* frame. MAAP and AAP proteins originating from this overprinting process, are found to play an important role in the viral life cycle (Chapter 3)[53,55].

Furthermore, the genome was discovered to be flanked by a 145 nucleotide-long inverted terminal repeat (ITR) (Figure 4)[35,38,51]. Analysis of these repeats revealed the first 125 nucleotides to have a multi-palindromic nature[35,38,51]. This means that the sequence of the termini is complementary to each other, allowing the DNA molecule to fold on itself, resulting in a T-shape hairpin structure (Figure 4B)[35,38,51]. The four subregions are denoted A, B, C, and D. B and C are asymmetric small internal palindromes that form the arms of the T structure. This T structure functions not only as an origin for DNA replication, by providing a free 3'hydroxyl group, but it is also essential for transcription, genome packaging, regulation, and site-specific integration during latent infection (Chapter 3)[35,38,51]. Therefore, the T-shape structure contains a Rep-binding element (RBE) and a terminal resolution site (trs) sequence for the Rep proteins to bind to and to fulfil their function[35]. Moreover, the other 20 bases of the ITR remain unpaired. This sequence is present only at each end of the genome and remains single-stranded[35,38].

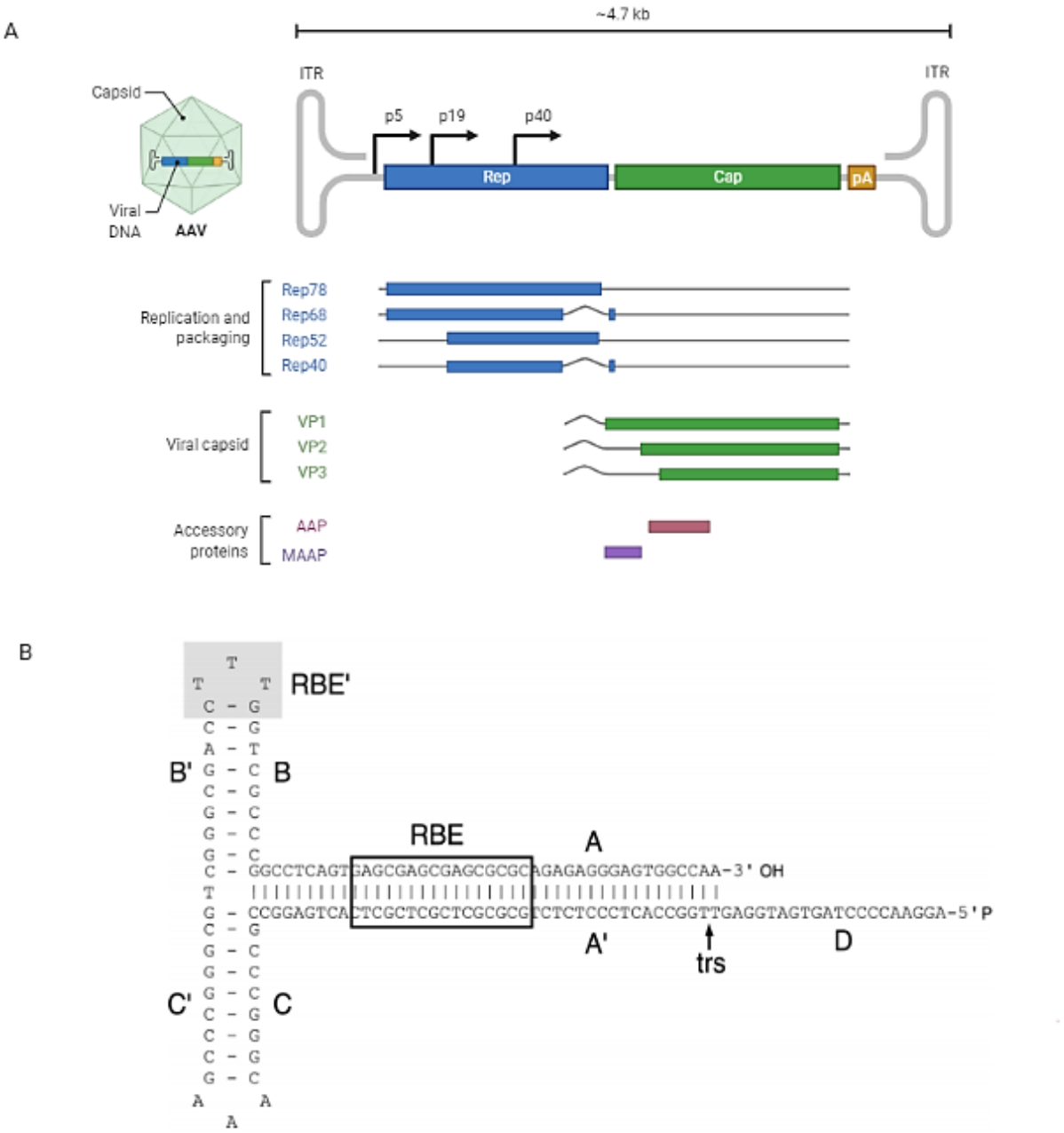

Figure 4: AAV2 genome and the secondary structure of the internal repeat. *(A) The AAV2 genome consists of four known ORFs; rep (blue), cap (green), MAAP (purple), and AAP (pink). The rep gene encodes for the Rep protein family and is regulated by the viral promotors p5 and p19 (arrows). The cap gene encodes for the structural viral capsid proteins VP1, VP2, and VP3 and AAP and MAAP, via (non)conventional start codons. This gene is under control of a single viral promotor; p40 (arrow). The AAV2 genome is flanked by an ITR, which functions as an origin of replication and is required for successful packaging, transcription, regulation, and insertion. The genome additionally contains a pA. Created with Biorender. (B) The ITR of AAV2 is composed of two palindromes (B'-B and C'-C) that are embedded in a larger stem palindrome (A'-A). The D sequence (D) reflects the remaining 20 base pairs that do not pair and remain single-stranded. The box motif and the shared nucleotides in the apex of the T-shaped structure, outline the Rep-binding element (RBE/RBE') where Rep proteins can bind. The RBE consists of a tetranucleotide repeat with the consensus sequence 5'GNGC'3'. The trs, necessary for DNA replication, is also depicted. Adapted from Gonçalves M (2005). AAV, adeno-associated virus; AAP, assembly activating protein; ITR, inverted terminal repeat; MAAP, membrane-associated accessory protein; ORF, open reading frame; pA, polyadenylation site; trs, terminal resolution site.*

2.4 Defining AAV serotypes

Thirteen different AAV serotypes (AAV1-AAV13) have been described for human and non-human primate sequences so far[57]. Noteworthy, a new serotype is defined as a newly isolated virus that

cannot be efficiently neutralised by antibodies specific for viral capsid proteins of all other existing and characterised serotypes[57,58]. Therefore, the distinction between serotypes can only be made if the newly isolated virus of interest has been tested with neutralising sera of all the characterised serotypes. When no serological difference can be found between any of the currently existing serotypes, the newly isolated virus is classified as a subgroup or variant of the corresponding serotype[57,58].

The AAV serotypes display different cell and tissue tropisms, low immunogenicity, sustained transgene expression, as well as transduction efficiency[59,60]. This difference can be attributed to variations in capsid surface topology, which determine the primary tropism as well as intracellular trafficking of the AAV (Chapter 2.2)[61]. Attachment to cell surface receptors is crucial for successful transduction (Chapter 3)[44,60,62].

The AAV capsids share a homology of ~60%-100% between serotypes. Differences in capsid sequence can be found in variable regions of the loops that form the majority of the capsid surface (see Chapter 2.2)[47–49]. These VRs are formed out of clustered monomers that form the 2/5-fold wall surrounding the depression, the top of three protrusions that surround the 3-fold axis, and the top of the channel at the five-fold axes (Figure 3)[40,46,47]. The variation in the surface loops, leads to distinct surface topology of AAV serotypes[47]. For example, variation in VRs could lead to differences in thickness and width of the 2/5-fold wall or to pointed or rounded protrusions affecting tissue tropism[47,57,60].

AAV serotypes appear to require specific recognition of different surface receptors for vector uptake and they display different transduction efficiencies in the same tissues (Figure 5)[5]. Therefore, the structural topology of the VPs alone cannot determine the receptor binding or transduction phenotypes. The amino acid composition and structural topology must also encode several important functions, including tissue tropism, transduction efficiency, and antigenic responses against the capsid proteins[47,57,60].

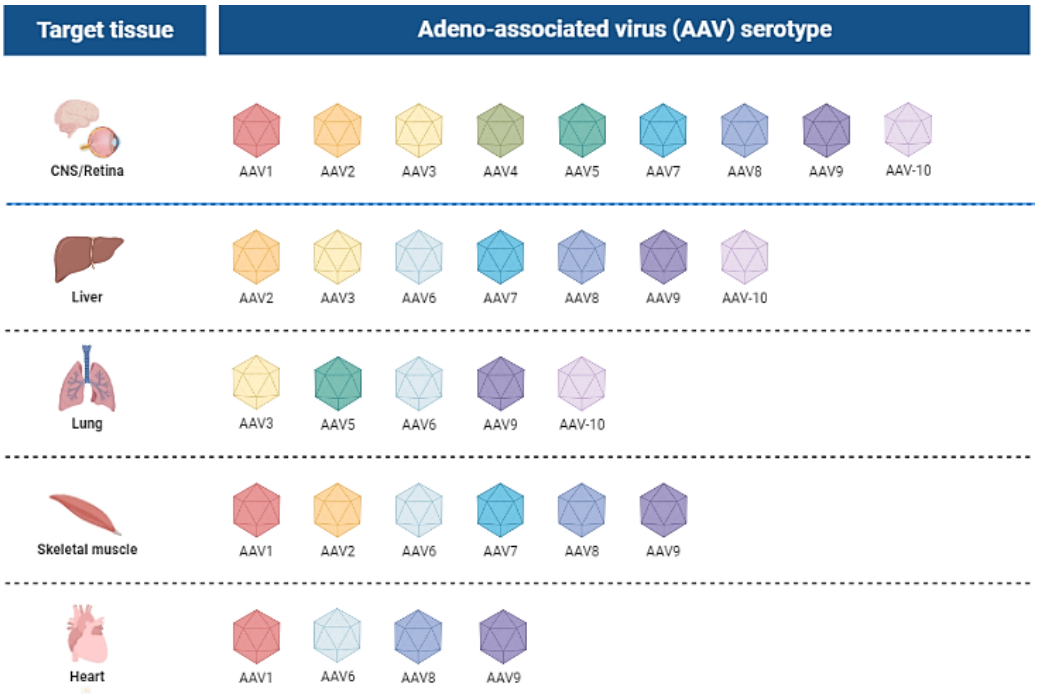

***Figure 5: Tissue tropism of AAV serotypes**. The figure depicts the target tissue of AAV serotypes for CNS/Retina, liver, lung, skeletal muscle, and heart[57,62]. AAV, adeno-associated virus; CNS, central nervous system. Adapted and adjusted from BioRender templates.*

Chapter 3: The AAV life cycle

AAV viruses have a unique mechanism of replication. These viruses reproduce, when a helper virus induces S phase in the host cell and provides components that promote gene expression and replication. When no helper virus is present, AAVs can establish a latent infection. The inactive genome can be activated upon subsequent infection of a helper virus (Chapter 3.6)[37,44].

The viral life cycle consists of six stages; attachment to the target cell, passage of the host cell membrane, uncoating, replication, assembly of the virion, and release of new viral particles (see Figure 6)[37,44]. Each stage is discussed thoroughly in this chapter.

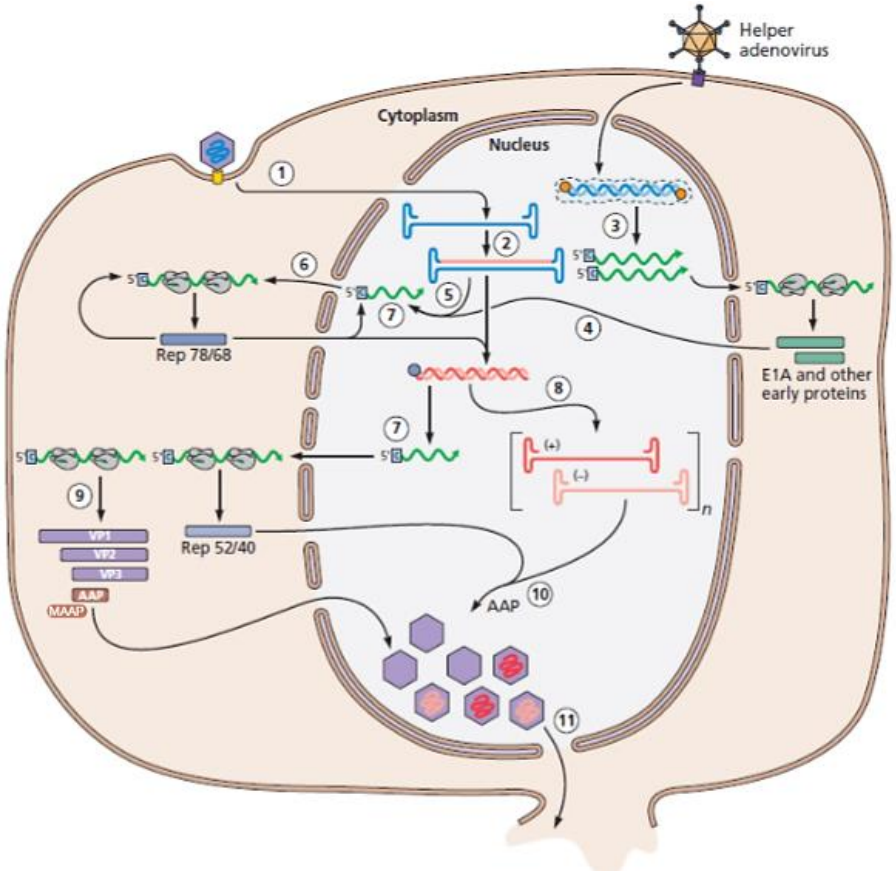

Figure 6: Viral life cycle of AAV. *AAVs bind to receptors on the host cell, which differ for different serotypes. (1) The process of adsorption, uncoating, and entry of the DNA into the nucleus. (2) The single-stranded viral DNA genome is converted to a large double-stranded molecule by cellular replication proteins. (3) AAV undergoes successful replication upon co-infection of a helper virus. The helper adenovirus produces early genes E1A, E1B, E4, and E2A which induce S-phase in the host cell and provide components needed for viral DNA expression and synthesis. (4) Transcription from the p5 promotor is also induced by the adenovirus E1A transcriptional activator, (5,6) leading to the production of Rep78/68 mRNA and proteins. (7) The Rep78/Rep68 proteins function as powerful transcription activators and induce transcription from p5 and p19 promotors. (8) Replication of viral DNA by single-strand displacement mechanism, which is initiated by recognition of the trs by Rep78/Rep68. (9) The capsid proteins, formed in the cytoplasm, self-associate in the nucleus with the help of AAP. (10) Newly synthesised virus particles are encapsidated. (11) Virus particles are released from the cell, usually via the destruction of the cell. Adapted and adjusted from Skalka et al. (2015). AAP, assembly-activating protein; AAV, adeno-associated virus; MAAP, membrane-associated accessory protein; trs, terminal resolution site; VP, viral capsid protein.*

3.1 Binding of AAV to target cells

Before the AAV viral genome can be introduced into the host cell, the virus has to cross the plasma membrane first. Therefore, the first step of viral entry is to attach to the target cell, which is initiated by the interaction of the capsid with cell surface receptors[44,60]. AAVs use specific glycans or glycoconjugates for cell binding and this interaction allows AAV particles to accumulate on the cell surface and gain access to proteinaceous (protein-like) co-receptors[60]. Binding to primary receptors

induces conformational changes in the AAV capsid that sets it into a favourable conformation that allows binding to co-receptors[63]. Binding to the co-receptors leads to internalisation of the virus[63].

To date, it has been discovered that AAV serotypes use 23 different glycan receptors to enter the host cell, giving rise to their distinct tissue tropisms[60]. These receptors can be grouped into three categories: The membrane-associated heparan sulphate proteoglycan (HSPG) was shown to be the primary attachment receptor for AAV2, AAV3, AAV6, and AAV13[43,60,62]. O- and N-linked sialic acid moieties are the primary attachment factors for AAV1, AAV4, AAV5, and AAV6. AAV9 uses N-linked galactose and glycan usage of AAV7, AAV8, and AAV10-12 is currently unknown[43,60].

Post attachment, interactions with secondary co-receptors are needed for vector internalisation via endocytosis and this process dictates the intracellular trafficking pathway and biological fate of the capsid (Chapter 3.2 and 3.3)[43,57,60]. Several co-receptors have been identified for numerous AAV serotypes (Table 1)[57,60].

Table 1: Proteinaceous co-receptors that are used by AAV serotypes for cell transduction.

Proteinaceous receptor	**AAV serotype**
αvβ5 integrin	AAV2
α5β1 integrin	AAV2
FGFR1	AAV2, AAV3
c-MET	AAV2
CD9 tetraspanin	AAV2
LamR	AAV8, AAV2, AAV3, AAV9
PDGFR	AAV5
EGFR	AAV6
AAVR	AAV1, AAV2, AAV5, AAV6, AAV8, AAV9

Abbreviations: AAVR, adeno-associated virus receptor; c-MET, hepatocyte growth factor receptor; EGFR, epidermal growth factor receptor; FGFR1; fibroblast growth factor receptor-1; LamR, laminin receptor; PDGFR, platelet-derived growth factor receptor. Information adapted from Pillay et al. (2017) and Wu et al. (2006).

3.2 AAV endocytosis

Upon attachment of the virion to (co-)receptors, AAV particles can be internalised via a variety of mechanisms[63]. The mechanism of endocytosis is most likely serotype and cell-type dependent[63]. Thus far, the endocytic process of AAV infection has only been studied for AAV2 and AAV5. At first, it was believed that AAV2 internalisation proceeds via dynamin-dependent mechanisms, such as clathrin-mediated endocytosis[64]. However, inhibition of dynamin did not lead to complete blockage of AAV2 endocytosis (70%), indicating alternative entry routes[64]. Two additional pathways used by AAV2 are caveolar endocytosis and micropinocytosis (Figure 7)[57,60,65]. The latter is a bulk fluid endocytic mechanism that is independent of clathrin and dynamin, but dependent of GTPase Rac1[64]. However, these entry routes do not equally lead to efficient transduction of AAV particles, because these endocytic vesicles follow unproductive trafficking routes within the cytosol[57,60,65].

It has been found that the most productive endocytic pathway appears to occur through clathrin-independent carriers and GPI-anchored-protein-enriched early endosomal compartment (CLIC/GEEC) pathway[57,60,63,65]. This pathway is mediated by uncoated tubulovesicular primary carriers (CLIC) that arise directly from the plasma membrane[64–66]. The carriers mature into tubular early endocytic compartments called glycosylphosphotidylinositol-anchored-protein-enriched compartments (GEECs)[66]. These compartments are organised at the plasma membrane into cholesterol-dependent

nanoscale clusters by the activity of cortical actin. The formation of endocytic tubules for AAV uptake is tightly regulated by membrane cholesterol, ADP-ribosylation factor 1 (Arf1), and cell division control protein 42 homolog (Cdc42), which are all critical components of the CLIC/GEEC pathway[63,65,66]. The GEECs subsequently fuse with sorting endosomes. Blockage of both CLIC/GEEC- and dynamin-dependent endocytosis resulted in complete blockage of AAV entry[57,60,65]. Thus, both dynamin dependent and dynamin-independent uptake routes are known for AAV entry, but endocytosis via the CLIC/GEEC pathway results in the most efficient transduction route[57,60,65].

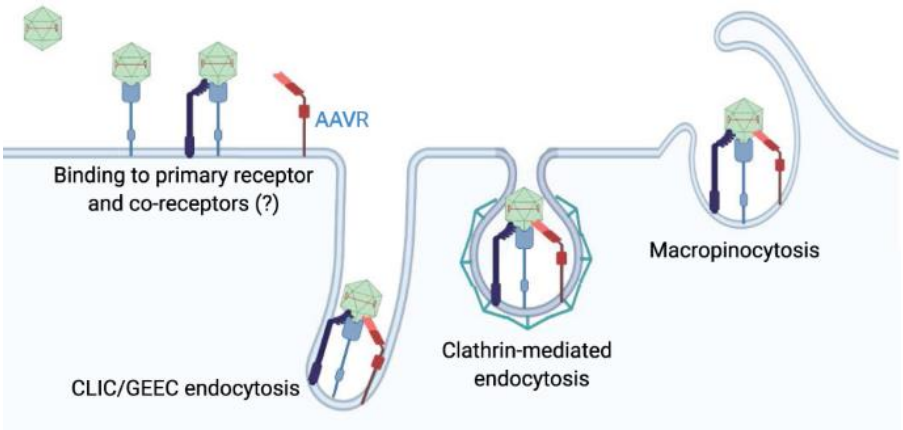

Figure 7: Endocytic routes of AAV into the cell*. The initial step of cell entry is attachment of AAV to its serotype-specific primary promotor (light blue). Hereafter, AAV interacts with a co-receptor (dark blue), of which AAVR is the main co-receptor for many serotypes. At least three different mechanisms of endocytosis have been proposed; clathrin-mediated endocytosis, micropinocytosis, and GLIC/GEEC pathway. Adapted from Riyad et al. (2021). AAV, adeno-associated virus; AAVR, adeno-associated virus receptor; CLIC/GEEC, clathrin-independent carriers and GPI-anchored-protein-enriched early endosomal compartment.*

3.3 Endocytic trafficking and endosomal escape

Following endocytosis, each endocytic vesicle contains one AAV particle that can follow several trafficking patterns to pass through the endosomal network[35,63]. Some of these routes ultimately lead to successful transduction, while others result in degradation of AAV capsid and genome[63–65]. The factor influencing successful transduction, was discovered after the observation that disruption of the Golgi apparatus structure completely abolished AAV2 transduction[63–65]. Hereby, it was found that in order to reach efficient transduction, AAVs must reach the perinuclear region via the Golgi apparatus (Figure 8)[63–65].

Normally, the sorting of endocytic cargos into different trafficking routes is determined by specific signals in the cytoplasmic tail of transmembrane receptors. However, despite their differences, the AAV serotypes appear to converge into a single retrograde transport pathway towards the trans Golgi network (TGN)[63,65]. Early endocytic vesicles are rapidly acidified after endocytosis, dependent on the depletion of endosomal calcium. Due to this, proteolytic cleavage of AAV capsid proteins by endosomal proteases occurs and this triggers extrusion of the PLA2-containing region of the VP1 capsid protein (VP1u) and VP2[45,47,63,67]. Normally, the PLA2 domain is buried inside the AAV capsid, blocked by channel forming amino acids (Chapter 2)[47]. Acidification of the endosomes, exposes the domain through pores that are located at the five-fold symmetry axis of the capsid[45,67]. The exposed PLA2 domain is kept enzymatically inactive, due to active export of calcium ions from the endosomal lumen. The vesicles are then transported to the TGN along a syntaxin 5 (STX5) dependent retrograde trafficking pathway[65]. This network contains a calcium-rich environment with a concentration near the optimal level for VP1-PLA2 activity. PLA2-activation induces viral escape into the cytosol, followed by nuclear import[63,65].

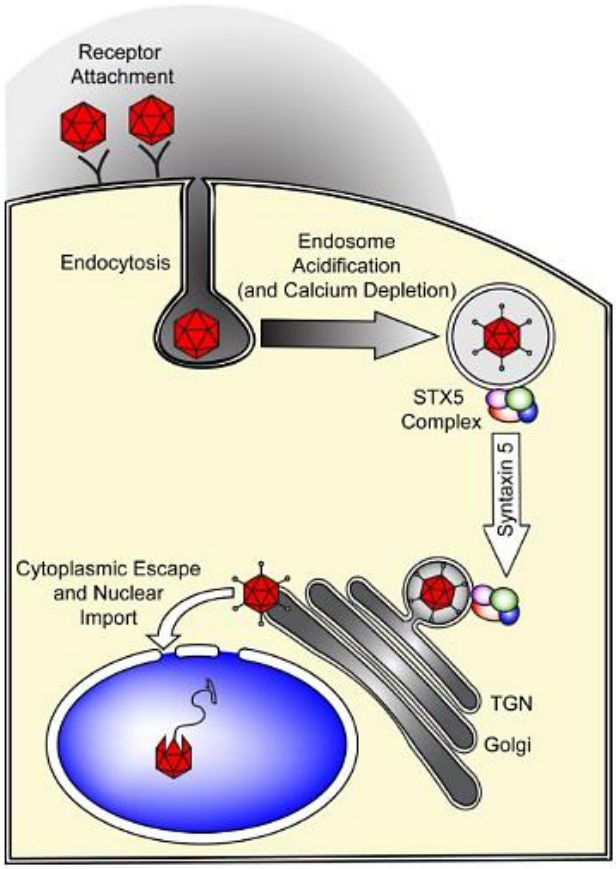

Figure 8: Syntaxin 5-dependent transport of AAV particles to the TGN/Golgi apparatus. *AAV particles bind to serotype-specific surface (co-)receptors, leading to endocytosis. Early endocytic vesicles are rapidly acidified, dependent on calcium depletion. The acidic environment, in combination with proteolytic endosomal proteases that cleave AAV capsid proteins, leads to the extrusion of the PLA2-containing domain of the VP1 capsid protein. The PLA2 domain is kept enzymatically inactive due to minute calcium concentrations in the endosome. AAV is transported to the TGN via syntaxin 5-dependent retrograde transport. Calcium concentrations within the TGN are near the optimal concentration for VP1-PLA2 activity. PLA2 activity allows AAV escape into the cytoplasm, followed by nuclear import and uncoating of the AAV capsid. Adapted and adjusted from Nonnenmacher et al. (2015). AAV, adeno-associated virus; TGN, trans-Golgi network.*

3.4 Nuclear import

After endosomal escape, the AAV capsid switches from trafficking route to the nucleus. How this process occurs exactly, remains unclear[63]. The AAV enters the nucleus with an intact capsid and this step is seen as the rate-limiting factor of infection[63,67]. After 16-20 hours of helper-free infection, only a limited number of AAVs can be found inside the nucleus[68]. Although entry of the particles through nuclear pore complexes (NPC) takes barely 12 milliseconds (ms), only 17% of the AAV virions that dock to this complex are actually imported[63,67,68]. This reveals that NPCs provide a strict selective step for AAV delivery [63,67,68]. Nuclear import is mediated by three classical nuclear localisation sequences that are imbedded in the VP1/VP2 common region (Chapter 2). The nuclear transport receptor importin β1 can bind to these sequences and regulates nuclear import[47,63,68]. After entering the nucleoplasm, virions transit through the nucleolus and enter the nucleoplasm again[63,69]. The exact role of this phase is not known, but it has been shown that the virions interact with nucleophosmin (NPM) and nucleolin in the nucleolus[69]. NPM stimulates Rep78-specific binding to the AAV ITR, as well as endonuclease activity. This suggests a role of this protein in AAV amplification, affecting Rep function and virion assembly[69]. Moreover, it was found that AAV capsids bind specifically to the major nucleolar phosphoprotein nucleolin[63,70]. It is suggested that nucleolin plays a key role in AAV replication, particularly in capsid assembly[70]. Taken together, this nucleolus step is found to be crucial for efficient cell transduction, provided that it is transient[63].

3.5 Genome release and uncoating

The process of AAV uncoating and genome release is poorly understood. Currently, it has only been studied in cell free systems and under non-physiological conditions[63]. The uncoating efficiency is most likely impacted by capsid stability[63,71]. Two alternative pathways have been proposed that explain genome release from the AAV capsid: (i) The capsid remains intact and the single-stranded (ss) DNA genome is ejected, (ii) The capsid is disassembled, leaving the ssDNA genome in a compact entangled conformation[47,71]. However, this mechanism remains enigmatic.

3.6 Genome replication or integration

After uncoating, AAV can follow either one of two distinct and interchangeable pathways of its life cycle: the replication productive cycle, known as the lytic stage, or the latent cycle named lysogenic stage[35,47]. The lytic stage develops in cells that are co-infected with a helper virus, whereas the latter is established in host cells in absence of a helper virus.

3.6.1 The lysogenic stage of the AAV life cycle

When a human cell is solely infected by AAV, the gene expression program of the virus is auto-repressed (Figure 9)[35]. There is limited AAV replication, repressed viral gene expression, and specific integration into the host genome[38]. Preferential integration of the AAV genome into a region of the human chromosome 19 ensures latency of the AAV virus[35,38]. This single preintegration region consists of roughly 2-kb and can be found on the chromosome's long arm (19q.13.4), which is known as *AAVS1*[72]. This region contains a sequence where Rep proteins can specifically bind to, which consists of the same tetranucleotide repeat that can be found in the RBE of the ITR (see Chapter 2.2)[35,38,72]. The Rep protein tethers the AAV genome to the *AAVS1* chromosomal sequence, by secondary structure and sequence-specific DNA binding. Moreover, binding of Rep78 and Rep68 to RBE leads to suppressed transcription. Genome integration of AAV enables perpetuation of the provirus DNA through host cell division[35,38]. The provirus DNA can be activated upon co-infection of the host cell with a helper virus, leading to genome expression and generation of new virus particles[35,38].

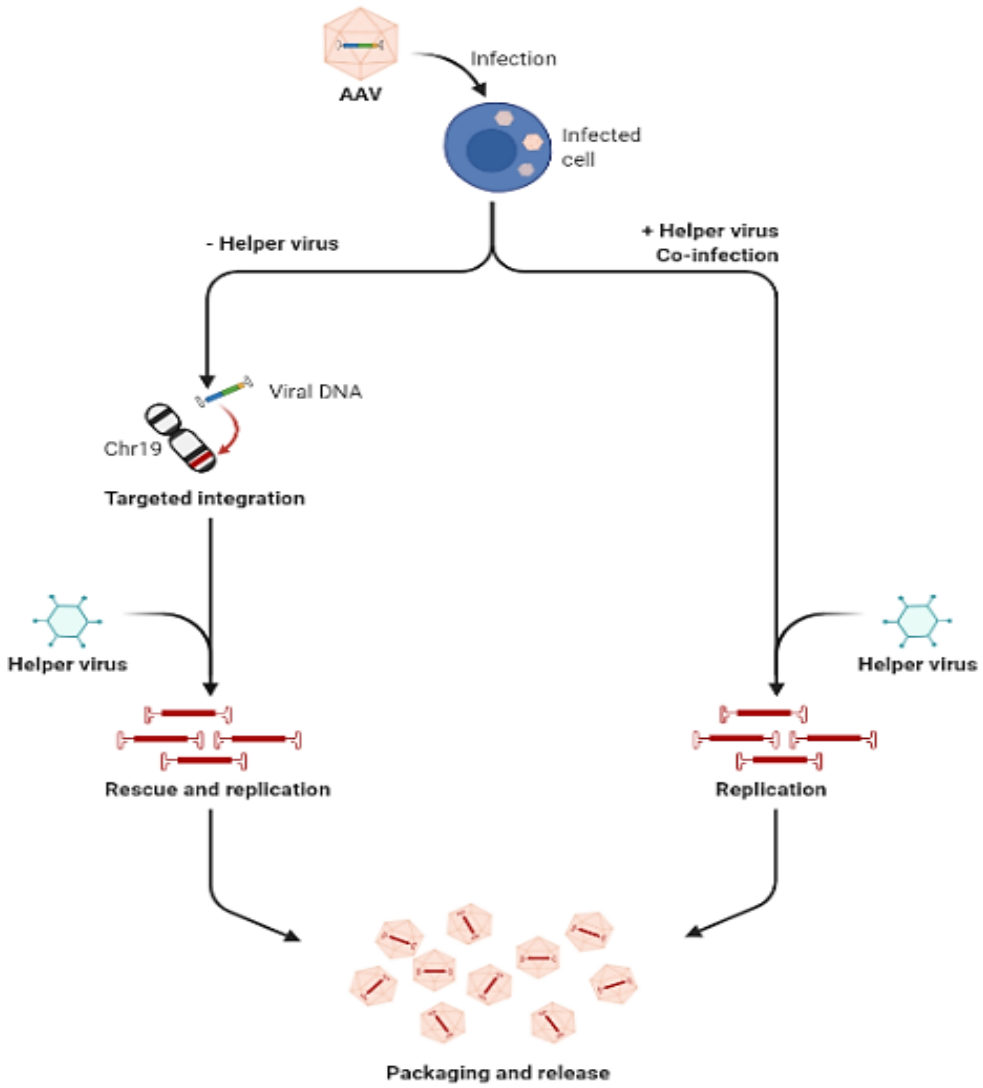

Figure 9: AAV life cycle with and without the presence of a helper virus. *Whenever a cell is infected with AAV, the virus can follow one of two pathways. (Left) In absence of a helper virus, AAV integrates in the AAVS1 region of chromosome 19 and is auto-repressed. Upon co-infection of a helper virus, proviral DNA is rescued and gene expression is activated. This leads to production of new virus particles and release. (Right) When an AAV infects a cell that is co-infected with a helper virus, gene expression is immediately activated. The AAV life cycle is started, leading to the production of new virus particles and release. AAV, adeno-associated virus. Adapted and adjusted from BioRender templates.*

3.6.2 The lytic stage of the AAV life cycle

When a latent infected host cell is co-infected with a helper virus, the AAV gene expression program is activated. This program leads to Rep-mediated excision of the provirus DNA from the host cell chromosome, which is followed by productive replication of the viral genome (Figure 9)[38,72].

3.6.2.1 Genome replication and generation of mRNA templates

After excision or introduction of the viral genome (in an already helper virus infected cell), the ssDNA genome is converted into a double-stranded form to allow transcription. The conversion of the genome occurs via a self-priming single-strand displacement mechanism (Figure 10)[35,47,71]. This mechanism is initiated by the T-shape structure of the viral genome. This structure provides a free 3'hydroxyl group that functions as a primer for host DNA polymerase[35,73]. The 3'ITR primer is elongated and hereby displaces and replicates the ITR at the 5'end (10.1). This leads to the formation of a linear double-stranded molecule (duplex monomer) with only one covalently closed end that is a prerequisite

for gene expression of the viral genome (10.2)[35,73]. The duplex monomer refolds into a double-hairpin configuration, aided by host or viral DNA helicases (10.3). Subsequently, a new 3'ITR primer is formed for DNA synthesis. While the 3'primer is elongated and displaces the complementary strand, AAV Rep78/68 proteins recognise and bind to the ITR at the downstream end. These proteins catalyse the resolution of closed termini by site-specific nicking of the trs of the downstream ITR (10.4)[35,47,71]. This initiates a second DNA replication complex, which allows DNA synthesis of the ITR before it is reached by the complex that is initiated on the other site. The first replication complex completes the replication to the end of the genome, by displacing the daughter strand (10.5 monomer). The recreated duplex monomer functions as a template for isomerisation again (10.6 monomer), whereas the displaced strand is packaged into the AAV capsid (10.7 monomer)[35,47,71].

When nicking by Rep proteins does not occur before the ITR is reached by the other replication complex, elongation proceeds through the ITR and the displaced strand (10.5 dimer/ 10.6 dimer). Hereby, dimeric genomes are generated. A new round of DNA synthesis can be initiated either by isomerisation of the open end by Rep endonuclease or by terminal resolution of the resolved end (10.7 dimer/ 10.8 dimer). Replication of the dimeric templates leads to displacement of single-strand dimeric inverted repeat genomes (10.9 dimer). This genome can then be packaged into the AAV virion (10.10 dimer)[35,47,71].

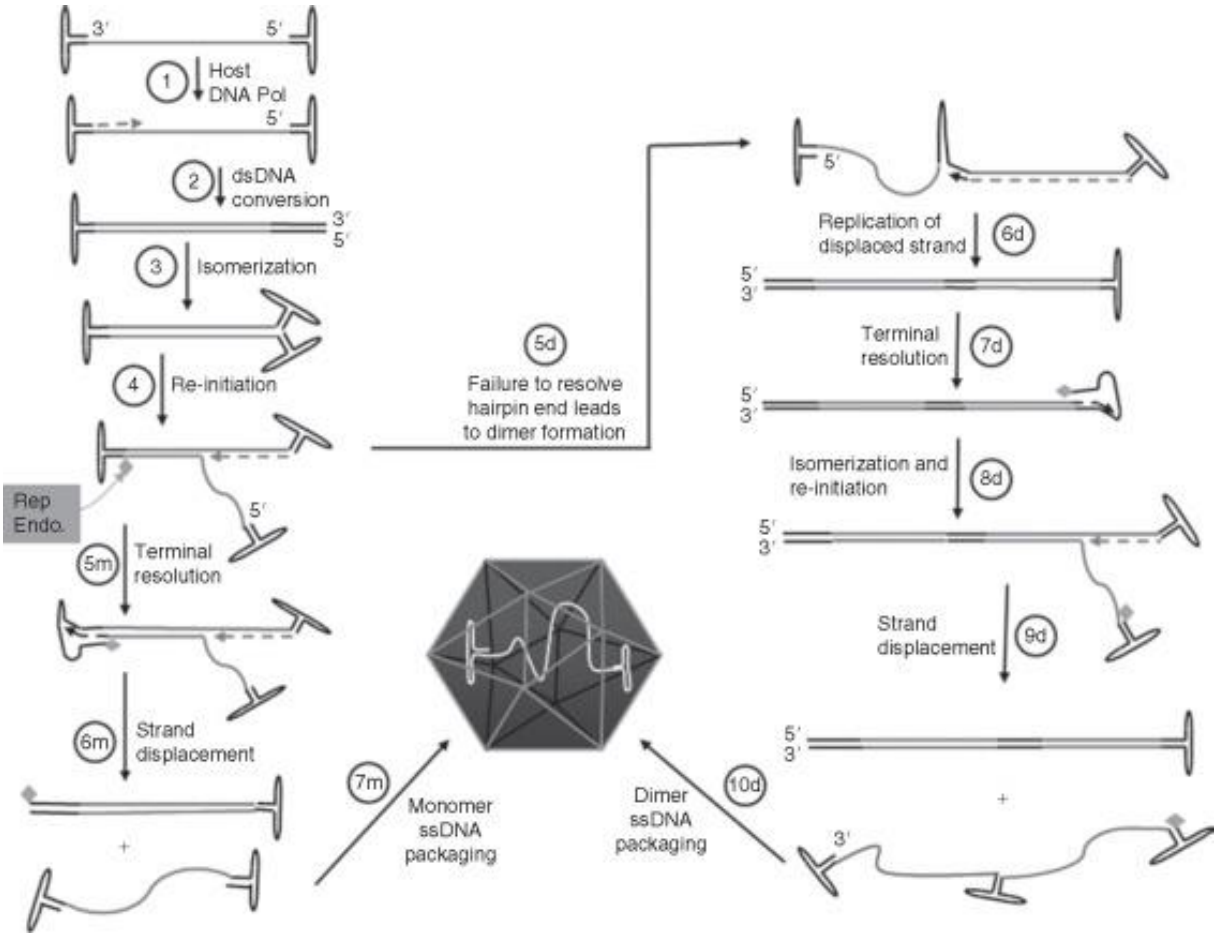

Figure 10: Schematic representation of AAV replication model. *AAV replication occurs via a self-priming single-strand displacement mechanism, which is initiated by a free 3'hydroxyl group. Host DNA polymerase can bind this primer site and initiate DNA synthesis (1). This leads to formation of linear double-stranded molecules/duplex monomers that contain one covalently closed end. This molecule functions as a prerequisite for gene expression (2). The duplex monomer refolds, generating a new 3'ITR primer for DNA synthesis (3). Upon 3'primer elongation and displacement of the complementary strand, AAV Rep78/68 proteins resolve the closed termini by site-specific nicking of the trs (4). This initiates a second DNA*

replication complex, allowing DNA synthesis of the ITR before it is reached by the other replication complex. The first replication complex completes DNA replication by displacing the daughter strand (5m) and the recreated duplex monomer functions as a template for isomerisation again (6m). The displaced strand is packaged into the AAV capsid (7m). When nicking of the trs does not occur before the ITR is reached by the other replication complex, elongation proceeds through the ITR and the displaced strand (5d/6d). This leads to generation of dimeric genomes which can be resolved either by isomerisation of the open end by Rep endonuclease or by terminal resolution (7d/8d). Replication of the dimeric templates leads to displacement of single-strand dimeric inverted repeat genome (9d), which is packaged in the AAV virion (10d). Adapted from McCarty (2008). AAV, adeno-associated virus; d, dimer; ITR, inverted terminal repeat; m, monomer; trs, terminal resolution site.

3.6.2.2 Genome expression

When the ssDNA genome is converted into double-stranded DNA, the viral genome can be transcribed[36,42]. Co-infection of a helper virus, alters the cellular environment and hereby aids in AAV gene expression[42]. The best studied AAV helper virus is the adenovirus type 5 (hAdV5), but other viruses such as herpes simplex virus, vaccinia virus, and cytomegalovirus were also shown to display helper functions for AAV[42]. The AdV genome encodes approximately 40 proteins that are divided into an early (E) and late (L) phase. The expression of these genes is tightly regulated and the minimal set of AdV helper factors needed for efficient AAV replication consists of five molecules: E1A, E1B55K, E2A, E4orf6, and VA RNA (Table 2)[36,42].

Table 2: Adenovirus helper factors that facilitate AAV replication and gene expression

Helper virus genes	Function
E1A	Relieving the repression of AAV p5 promotor, hereby activating AAV Rep78 and Rep68 protein expression.
E2A	Stimulation of AAV DNA replication and involved in splicing of Rep40 and Rep68 proteins.
E1B55K and E4orf6	Complex promotes AAV second-strand synthesis and viral DNA replication. E1B55K facilitates AAV mRNA export and inhibits cellular mRNA export. Consequently, more cellular machinery/proteins are available for AAVs life cycle.
VA RNA	Stimulates AAV protein expression, cap expression, and assembly.

Abbreviations: E1A, adenoviral early 1a gene; E1B55K, adenoviral early gene; E2A, adenoviral early 2a gene; E4orf6; adenoviral early gene; VA, adenoviral viral associated. Information generated from Meier et al. (2020) and Balakrishnan et al. (2014).

3.7 Genome packaging and virion release

After generation of new ssDNA genomes, the genomes need to be enclosed in a preassembled AAV capsid. This process occurs in the nucleus and is supported by AAP[74]. The exact mechanism by which AAP aids in capsid assembly has yet to be elucidated, but ideas about this process have been proposed[74,75]. In 2015, Earley *et al*. identified nuclear and/or nucleolar localisation signals in the AAP C-terminus and proposed AAP to promote translocation of VP3 proteins to the nucleus for AAV2[74,76]. Furthermore, it was suggested by Naumer *et al.* that AAP induces a conformational change in VP3, indicating a function as scaffold that nucleates capsid assembly[74,77]. Moreover, it might also remain possible that AAP promotes nucleolar VP transport to facilitate interaction with nucleolar proteins that chaperone AAV capsid assembly, such as nucleolin. However, it was demonstrated that assembly of other AAV serotypes can occur outside the nucleolus. Therefore, it can only be stated that AAV capsid assembly is supported by AAP and that its requirement ranges broadly across serotypes[74–77].

Newly synthesised DNA needs to be enclosed into the preassembled capsid[42,78]. This occurs via 12 channels that are displayed at the fivefold axes of symmetry of the capsid structure (Chapter 2)[78]. These channels function as portals through which AAV ssDNA can be taken up[78]. For this process, helicase activity of the small Rep40 and Rep52 proteins is required[78]. These proteins function as motors to translocate AAV genomes into the preformed empty capsids[79]. Furthermore, it is suggested that a large Rep protein that is covalently attached to newly generated AAV genomes, might serve as a packaging signal for genome encapsulation. This hypothesis arose after the discovery that *rep-cap* sequences can still be packaged in the absence of the ITRs, whenever the genome is bound by Rep[42,80].

After the generation of new AAV particles, the progeny virions need to exit the host cell to complete the infectious life cycle[37]. This happens via cell lysis, which is not induced by AAV but by CPE from the co-infecting helper virus[37]. The exact mechanism by which a helper virus, such as adenovirus, induces cell lysis remains to be elucidated.

Thorough understanding of the steps within the AAV life cycle has guided the discovery of AAV's therapeutic potential and this has driven the development of recombinant AAVs (rAAVs) which are promising tools for gene therapy.

Chapter 4: Gene therapy using recombinant adeno-associated viruses and clinical applications in heart failure

Gene therapy has gained significant momentum over the past few years[61]. This therapy introduces foreign genetic material into target cells, via non-viral or viral vehicles, in order to treat or prevent diseases by correcting or delivering defective genes[61]. In 1984, Hermonat *et al*. were the first to demonstrate that AAVs can be used to transduce foreign DNA into human and murine tissue culture cells and this pioneered AAV gene therapy[7]. Since then, AAV vectors emerged as the most efficient viral vectors for this therapy and numerous studies have been carried out to create and optimise promising AAV vector systems for gene therapy in humans[36].

4.1 The design of AAV recombinant vectors

Recombinant vectors are defined as vectors that express a transgene of interest and that have lost the ability to replicate[81]. In order to use AAVs as such a gene delivery vehicle, several considerations need to be made. These include the ability to attach and enter the target cell, successfully transfer towards the nucleus, express the genome for a sustained period of time, and to display a negligible amount of toxicity[38]. AAVs are successful in fulfilling all of these criteria and several concerns have guided the development of current AAV vectors.

Concerns about the size and integration potential of the AAV genome, have led to the construction of a rAAV that does no longer encode the RBE sequence[38,81]. This sequence is required for site-specific integration during lysogenic stage (Chapter 3)[38,81]. Therefore, rAAVs can only persist as a circular episomes in the nucleus that drive transgene expression[63]. These episomes can concatemerize, forming high molecular weight structures that are maintained extrachromosomally[63]. Moreover, the rAAVs are created by excision of the entire *cap* and *rep* genes and by insertion of a transgene expression cassette smaller than 4.9 kb (Figure 11)[82]. This cassette is placed between the ITRs, which are the minimal *cis*-acting elements required to direct DNA replication and packaging[6,83–85]. Moreover, the choice of the right promoter (size, tissue specific, etc.), the gene of interest, the serotype, and the polyadenylation signal are essential for the rAAV design[83].

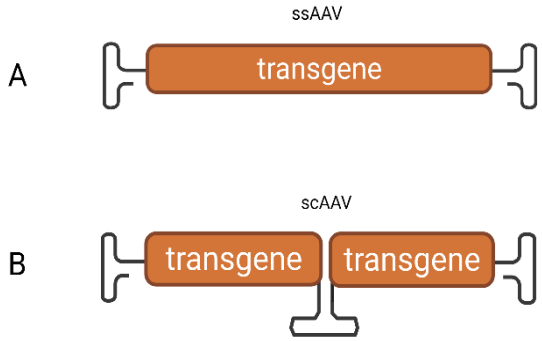

Figure 11: Construction of recombinant ssAAV and scAAV. *(A) The ssAAV is generated by excision of the rep and cap genes and insertion of a transgene expression cassette between the ITRs. (B) The scAAV is generated by the elimination of the trs in one of the inverted repeats, resulting in dsDNA with a self-complementary configuration. The rep and cap genes are excised and replaced by insertion of a transgene. AAV, adeno-associated virus; ds, double-stranded; ITR, inverted terminal repeat; sc, self-complementary; ss, single-stranded trs, terminal resolution site. Created with BioRender.*

Numerous changes to the capsid and transgene expression cassette have been developed in recent years in order to improve gene transfer efficacy and to evade the weak and highly transient innate immune responses[86]. This has led to another promising rAAV design: the self-complementary AAV (scAAV) (Figure 11)[83]. Because the ssAAV genome is single-stranded, it has to be converted to a double-stranded form in the nucleus for transgene expression to occur. This step is seen as a rate-limiting step of transduction and with the development of scAAV vectors, this step is bypassed[83,86]. These vectors are created by the elimination of the trs in one of the inverted repeats (Chapter 3), leading to double-stranded scAAV genomes with a self-complementary configuration. Upon uncoating of the viral particles in the cells, the scAAV immediately forms an intramolecular double-stranded DNA. Due to capsid space limitation, the size of the expression cassette has to be reduced to not exceed the packaging limit, so the scAAV can only carry half of the ssAAV genome[83,86]. This method is advantageous as it can bypass double-strand synthesis and its design leads to quicker expression kinetics and stronger expression levels than ss-rAAV[83,86].

4.2 Production strategies of rAAVs

The ability to produce high quantities of rAAVs is an important factor for the development of gene therapy-based medicines[87]. Currently, three expression systems are used for industrial rAAV production: adenovirus (AdV), herpesvirus (HSV), and baculovirus (BV) complementation systems[82]. The molecular design of the rAAV-producing systems plays a critical role in vector productivity per cell (vector genomes per cell), in process robustness, and in elimination of process and product-related impurities[82]. However, these systems are all based on the same basic molecular commonalities: (i) successful delivery and amplification of the transgene in the host cell line, (ii) fine-tuning of *Rep-Cap* expression levels, and (iii) modification of the cellular atmosphere to an AAV-friendly environment[82,88]. The set-up mechanism between these systems varies, but they are all fundamentally focussed on the knowledge that ITRs are the only *cis*-acting viral elements required for vector production and that the

Rep/Cap gene products and helper virus proteins can be supplied in *trans* with the use of separate constructs[82,88].

The most robust and versatile method to produce stocks of rAAVs utilises a three-component plasmid system: an AAV plasmid vector containing the transgene flanked by AAV ITRs; an AAV helper plasmid providing necessary capsid and replication proteins *in trans*; and an AdV, HSV, or BV helper plasmid providing helper genes (Figure 12)[82,88].

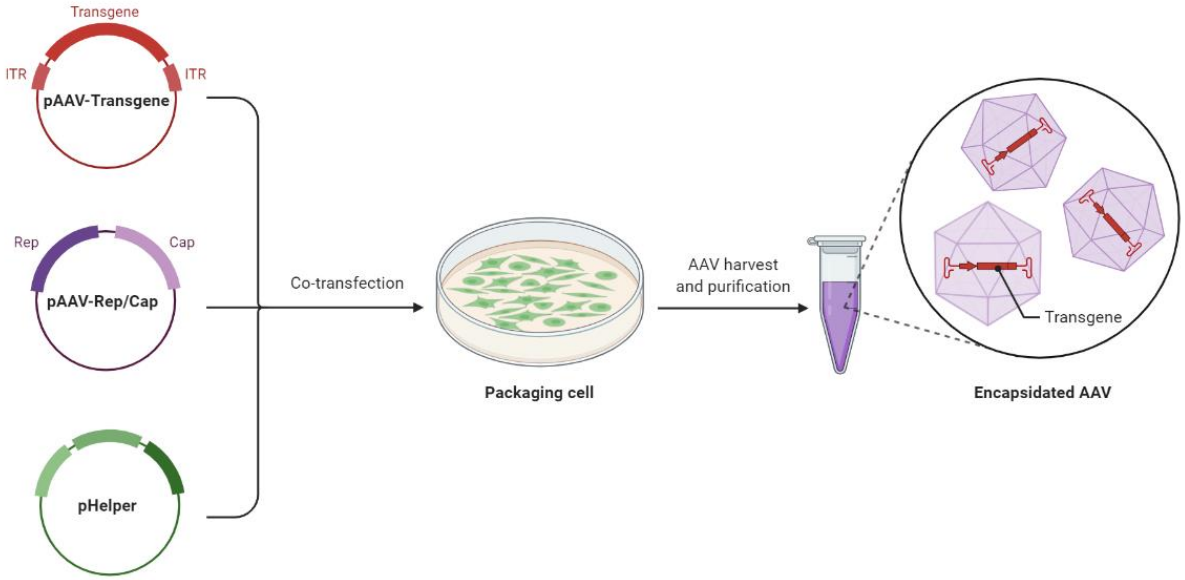

Figure 12: Overview of the most versatile method to produce rAAVs. *This method is based on a triple transfection method. A packaging cell line is transfected with a three-component plasmid system: (i) pAAV-transgene plasmid, which contains the transgene flanked by AAV ITRs, (ii) pAAV-Rep/Cap plasmid, which provides the rep and cap genes in trans necessary for AAV capsid and replication proteins, and (iii) pHelper plasmid, providing helper genes from either AdV, HSV, or BV. After co-infection of these plasmids into the packaging cells, the recombinant AAV vectors can be harvested and purified, resulting in isolation of encapsulated transgene AAVs. AAV, adeno-associated virus; AdV, adenovirus; BV, baculovirus; HSV, herpes simplex virus; ITR, inverted terminal repeat. Adapted and adjusted from BioRender templates.*

4.1.1 Adenovirus complementation system

This complementation system uses the three-component plasmid system with an Ad helper plasmid providing E2A, E4orf6, and VA RNA[88]. Notably, the absence of homologous sequence between the Ad helper plasmid and the transgene-construct reduces the risk of generating replication competent rAAVs[83]. The plasmids are co-transfected into human embryonic kidney (HEK) 293 cells, which already constitutively express the adenovirus proteins E1a and E1b[82]. The presence of the five aforementioned Ad helper proteins, leads to rAAV genome rescue from the plasmid backbone and to replication and packaging of the transgene into AAV particles (Figure 12)[35,81,88]. Subsequently, these particles can be purified from a cell lysate, using either anion exchange, affinity chromatography, or density gradient centrifugation techniques[89].

This complementation system is commonly adopted in lab settings, due to its simple rAAV production workflow, flexibility to switch production to different serotypes, and proven productivity and product quality[82]. However, this triple transfection method is unwieldy for large-scale vector production and has limited reproducibility[82]. Therefore, stable packaging and producer cell lines have been developed that form an alternative for these co-transfection techniques[88]. These cell lines contain integrated copies of *Rep/Cap* or *Rep/*Cap plus vector constructs into the cell genome[88]. They both still require the

addition of Ad helper genes via plasmid transfection or virus infection. With this methodology, scalability is improved and the number of required plasmids is reduced, resulting in vector genome titers ranging around 10^4-10^6 vector productivity per cell (vp/cell)[82].

4.1.2 Herpesvirus complementation system

The HSV system is an alternative platform that overcomes scale-up limitations identified with AdV-based systems, while maintaining high productivity at large scale[82,83]. The design of this system consists of two replication-deficient HSV strains that are engineered to individually harbour *Rep/Cap* and transgene sequences[82,83]. The two strains double infect a mammalian cell line, such as baby hamster kidney (BHK) or HEK cell lines. These cell lines are easier to scale up and they generate high yields ranging around 8 x 10^4 – 2 x10^5 vp/cell[82,83]. The main challenge of this system relies on viral inoculum stability and propagation, and therefore current research is focussing on improving this growth and stability in culture[82,83].

4.1.3 Baculovirus expression system

The BV expression system is one of the most promising methods to produce rAAVs and it was established by Urabe *et al.* in 2004[82,90]. This method is based on the infection of an insect cell line, *Spodoptera frugiperda 9* (Sf9), that is cultured in suspension with three recombinant baculoviruses[82]. The first BV contains the Rep78 and Rep52 genes, the second BV expresses the AAV capsid proteins and the last BV contains the ITR-flanked transgene[82,85]. This system's cell productivity is among the highest documented to date, namely >10^5 vg/cell[82]. This design supports the production of very efficacious, robust and scalable infectious rAAVs by reducing the number of required BVs. However, the instability of the BV is very challenging as it depends on the passage number of the insect cell[82].

4.3 Advances in AAV-mediated gene therapy for the suppression of heart failure

The recombinant AAVs are attractive for gene therapy for several reasons[6,7]. Among them are: (i) rAAVs are able to transduce a broad spectrum of proliferating and quiescent cell types[84]. (ii) In at least postmitotic cells, rAAVs lead to long-term transgene expression (expression for >1 year following a once-off delivery of AAV vector[5]) and this occurs even in absence of genome integration[82]. (iii) rAAVs have low immunogenicity due to the ITRs being the only required *cis*-elements and the lack of viral protein expression[82] and (iv) rAAVs can accommodate tissue-specific promotors[84].

One of the fields that is in desperate need for the development of new therapeutics, possibly using gene therapy, is for cardiovascular research and specifically for heart failure[6]. Currently, treatment options for HF are limited and focus on delaying disease progression and managing disease symptoms, rather than curing[5]. The largely non-dividing cardiac cells, named cardiomyocytes, are a promising target cell for recombinant AAV vectors[6]. Extensive research has been performed to test the potential of rAAVs for heart failure and a plethora of successful studies have been carried out, especially in rodents, but also in pre-clinical relevant large animal studies[5,6]. However, translating this success to large animal models and to clinical trials has proven to be more challenging[5,6].

4.3.1 Effect of PLN(R14del) on cardiac contraction

The global prevalence of heart failure is approximately 26 million patients and it is a leading cause of mortality in developed countries[3,4]. 36% of all heart failure cases can be attributed to dilated cardiomyopathy (DCM) as the underlying cause[3]. One of the main features of heart failure is a depressed contractility[4]. The key player in cardiac contractility as well as in coupling of excitation and contraction, is the sarcoplasmic reticulum (SR)[9,91]. The SR is accountable for calcium storage in

cardiomyocytes and the contractile force of these cells depends on the amount of Ca^{2+} that is accumulated within the SR. Therefore, regulation of intracellular Ca^{2+} is crucial for cardiac functioning and disruptions of this process can lead to cardiac failure[9,91].

In response to depolarisation of the cardiomyocyte membrane, Ca^{2+} enters the cytoplasm via voltage-gated Ca^{2+}-channels in the plasma membrane and binds to ryanodine receptors (RyRs) to stimulate Ca^{2+}-release from the SR (Figure 13)[91]. Ca^{2+} can then bind to troponin C in the thin filament, which in turn transmits information via structural changes throughout the actin-tropomyosin filaments[92]. Hereby, myosin ATPase activity and muscle contraction is activated[92]. Hereafter, Ca^{2+} has to be removed from the myoplasm to induce cardiac muscle relaxation[91]. This occurs via Ca^{2+}-ATPases, Na^{+}/ Ca^{2+} exchangers, or by sarco(endo)plasmic reticulum calcium ATPase 2a (SERCA2a). This pump is located in the SR and its activity accounts for >70% of Ca^{2+}-removal from the myoplasm in humans and for the accumulation of Ca^{2+} storage in the SR[91].

A transmembrane SR phosphoprotein, named PLN is a crucial protein that regulates Ca^{2+} cycling in cardiac muscle by interacting with SERCA2a (Figure 13)[9,91]. This protein exists in two oligomeric forms: (i) a monomer that directly binds to SERCA2a and inhibits it and (ii) a pentamer that indirectly influences SERCA2a activity by regulating the pentamer-monomer equilibrium[91]. PLN forms pentamers in SR membranes that dissociate into monomers upon SERCA2a interaction[93]. The interaction between PLN and SERCA2a is dependent on the phosphorylation state of PLN, which in turn determines the activation state of SERCA2a. In the dephosphorylated state, PLN monomers interact with SERCA2a and inhibit SERCA2a activity by decreasing its affinity for Ca^{2+}. Upon phosphorylation of PLN at Ser16 by protein kinase A (PKA) or Thr17 by calcium-dependent protein kinase II or protein kinase B, a conformational change in PLN is induced that abolishes the inhibitory interaction and restores the SERCA2a Ca^{2+} affinity[93,94]. In this stage, phosphorylation at either Ser16 or Thr17 leads to enhancement of PLN pentamers[93]. This results in an increased rate of cardiac relaxation and an increased cardiac contractility in proportion to the accumulation of Ca^{2+} storage in the SR[4,9,91,95].

In 20% to 40% of the patients with familial DCM and in 15% to 25% in unselected patients with DCM, underlying pathogenic variants can be found[3]. One of the pathogenic mutations in DCM was found in the *PLN* gene on chromosome 6. A deleterious mutation of the arginine 14 codon in the *PLN* gene (p.(Arg14del)) is associated with prevalent ventricular arrhythmias, contractile dysfunction, heart failure, and sudden cardiac death[9,10]. In contrast to wildtype PLN, PLN R14del does not undergo any conformational changes upon phosphorylation, resulting in inhibition of PLN pentamer formation and thus constitutive inhibition of SERCA2a, and dysregulation of the Ca^{2+} homeostasis (Figure 13)[96].

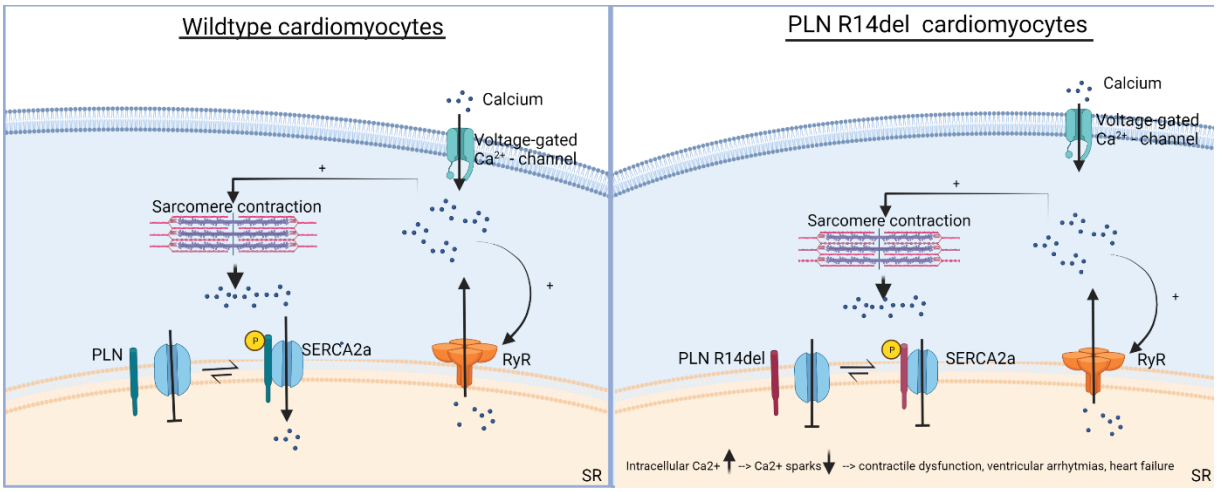

Figure 13: Mechanism of Ca^{2+}- cycling in cardiomyocytes upon depolarisation. *(Left) Upon depolarisation, Ca^{2+} enters the cardiomyocytes through voltage-gated Ca^{2+}- channels and binds to RyRs, stimulating Ca^{2+} release from the SR. Ca^{2+} activates sarcomere contraction in the cardiomyocytes and relaxation is induced by depletion of Ca^{2+} through predominantly SERCA2a. SERCA2a activity is regulated by the phosphorylation state of PLN. Dephosphorylated PLN inhibits SERCA2a activity by decreasing the pumps affinity for Ca^{2+}. Phosphorylated PLN abolishes the inhibitory interaction with SERCA2a and restores the Ca^{2+} affinity of SERCA2a, resulting in Ca^{2+} storage in the SR. This results in cardiac relaxation and storage of Ca^{2+} for a new round of cardiac contraction. (Right) A deleterious mutation of Arginine 14 codon in the PLN gene (R14del) results in a PLN protein incapable of abolishing the inhibitory interaction with SERCA2a upon phosphorylation. This results in constitutive inhibition of SERCA2a and no uptake of Ca^{2+} in the SR. The Ca^{2+} homeostasis is dysregulated, resulting in increased intracellular Ca^{2+}, decreased Ca^{2+} sparks during contraction, contractile dysfunction, ventricular arrhythmias, and heart failure. Ca^{2+}, calcium; PLN, phospholamban; RyRs, ryanodine receptors; SERCA2a, sarco(endo)plasmic reticulum calcium ATPase 2a; SR, sarcoplasmic reticulum. Created with BioRender.*

Currently, a proven effective treatment for patients harbouring the PLN mutation is lacking[11]. At this time, efforts to identify a tailored therapy are ongoing, using state of the art technology and through synergistic collaborations. The therapeutic research is divided into three different directions: (i) DNA; research towards correcting the PLN mutation in the DNA using DNA-editing techniques such as CRISPR-Cas and Prime Editing. (ii) RNA; research towards possibilities to block erroneous PLN R14del mRNA. (iii) Existing medication; research aimed at repurposing existing drugs as treatment for PLN. Within the first two subcategories, rAAVs are the leading platform for *in vivo* gene therapy delivery.

4.3.2 AAV gene therapy approaches on PLN(R14del)

Several experiments have pioneered the potential of PLN-modulation for heart failure, by determining the effect of different PLN-levels on cardiac muscle contractility[97]. When the Kranias group (2006) generated PLN-deficient mice, it was found that their hearts displayed enhanced myocardial performance without any deleterious side effects[4,98,99]. Moreover, Minamisawa *et al.* (1999) showed that reducing or eliminating PLN levels in murine models of dilated cardiomyopathy led to beneficial effects on cardiac failures[4,97]. Additionally, they showed that expression of a PLN point mutant dominantly activated contractility of the cardiomyocytes by interference of the PLN-SERCA2a interaction[97]. These findings suggested a new therapeutic target to enhance contractility in a failing heart, by modulating PLN levels to regulate calcium handling[4,97–99].

Several gene therapy approaches have been attempted based on this hypothesis. For example, Hoshijima *et al.* (2002) developed an *in vivo* rAAV transcoronary delivery system that allowed stable, highly efficient and cardiac-selective gene expression of a pseudo-phosphorylated mutant of human PLN (S16E)[100]. This mutant mimics the conformational change in PLN which is induced after PKA phosphorylation. The rAAV was delivered to BIO14.6 cardiomyopathic hamsters, which is a well-characterised hamster model of progressive heart failure with dilated cardiomyopathy[100]. The vector

was used to constitutively activate SR Ca^{2+}-cycling in the myocardium of the hamsters. The chronic inhibition of PLN by S16EPLN peptide resulted in an increase of cardiac diastolic and systolic function for over seven months and the S16EPLN was also capable of inducing stable activation of SERCA2a, which resulted in enhancement of cardiac relaxation and contractility[100].

These results hold promise for using rAAVs to treat PLN R14del patients as well. The CURE-PLaN network[101], in collaboration with the Dutch PLN Patient Foundation[102], are at the moment of writing, investigating several therapeutic approaches using AAVs as a gene delivery vehicle to cure PLN R14del (Table 3). Due to the fact that these approaches are currently under investigation and no preliminary data is available, a short overview of literature will be provided that might have supported the urge to explore these techniques for PLN R14del patients.

Table 3: Current investigations by CURE-PLaN to cure or treat PLN R14del mutations using AAVs as a gene delivery vehicle

CUREPLaN	Approach	Delivery	Stage
New york	CRISPR/Cas9	AAV	Murine
Amsterdam	siRNA KD R14del	AAV	iPS-CM; hECT
Groningen	ASO	AAV	Murine

Abbreviations: AAV, adeno-associated virus; ASO, antisense oligonucleotides; CRISPR/Cas9, clustered regularly interspaced short palindromic repeats and CRISPR associated protein 9; hECT, human engineered cardiac tissues; iPS-CM, human induced pluripotent stem cell-derived cardiomyocytes ; R14del, deleterious mutation of the arginine 14 codon in the PLN gene; siRNA, small interference RNA; KD, knockdown

4.3.2.1 CRISPR/Cas9

Currently, the effect of PLN R14del gene correction with CRISPR-Cas9 is under investigation. This approach might be beneficial, as this technique might provide new opportunities to study underlying mechanisms of the PLN R14del pathogenesis. A more thorough understanding of the disease might eventually enable the development of personalised therapies.

Karakikes *et al.* (2015) have modelled patient-specific human induced pluripotent stem cell-derived cardiomyocytes (hiPSC-CMs) that recapitulate the pathogenic PLN R14del disease phenotype and have used a genome engineering technique to correct the mutation[103]. When causative genetic mutations are present, three different types of molecular scissors are designed that can be used to cut at specific sites: (i) Zinc finger nucleases (ZFNs), (ii) transcription activator-like effector nucleases (TALENs), and (iii) CRISPR[104]. Karakikes *et al*. used the TALEN technique to correct the *PLN* mutation in hiPSC-CMs from a PLN R14del patient[104]. This technique is designed to introduce a double-strand break adjacent to the PLN R14del mutation. Subsequently, a gene correction matrix corrects the mutation for the wt*PLN* gene[104]. This genomic correction resulted in a full restoration Ca^{2+}-cycling[104]. Furthermore, they proved that knockdown of the endogenous *PLN*, while a codon-optimised human *PLN* is simultaneously expressed, reversed the disease phenotype *in vitro*[104]. For this approach, combinatorial AAV6-mediated gene therapy was used. This vector was designed with a scAAV genome, to knockdown the endogenous *PLN* by intronic artificial microRNA (miR-PLN), together with the overexpression of microRNA-resistant, codon-optimised PLN[104]. The scAAV genomes were packaged into AAV6 capsids, allowing high transduction efficiency of cardiac cells[104]. This approach resulted in ~50% knockdown of endogenous *PLN* transcripts and a very high expression of wtPLN[104]. This experiment revealed that the presence of wtPLN alone is sufficient to rescue impaired calcium handling characteristics in R14del-CMs *in vitro*, without the need to supress mutant PLN[104].

In vivo AAV-mediated correction has additionally been performed in murine models to study hypertrophic cardiomyopathy (HCM) and to study frame-shift mutations associated with HCM[105,106].

These studies have yielded results proving efficacy in reversing myocardial fibrosis for ~six months and prevention of cardiac hypertrophy and dysfunction for a period of 34 weeks[105,106].

All the aforementioned experiments prove significant potential to investigate this gene therapy approach based on AAV-mediated delivery *in vivo* in an appropriate PLN R14del murine model of DCM. Recently, the CRISPR/Cas9 genome editing tool has supplanted the TALEN and ZFN technique, due to its greater efficiency and ease of use[107]. This technique is composed of a Cas9 enzyme that cuts DNA at specific sites, directed by guide RNA (Figure 14)[107]. It creates a double strand break and this induces a DNA repair response through one of two mechanisms: error prone non-homologous end joining or, in the presence of a homology template, accurate homology-directed repair (HDR)[107]. The latter mechanism is used for precise gene editing of the target locus, by providing a repair template. Using a PLN repair template to correct the endogenous *PLN* for wt*PLN* in murine models, may lead to new insights that may pave the way for development of new therapies.

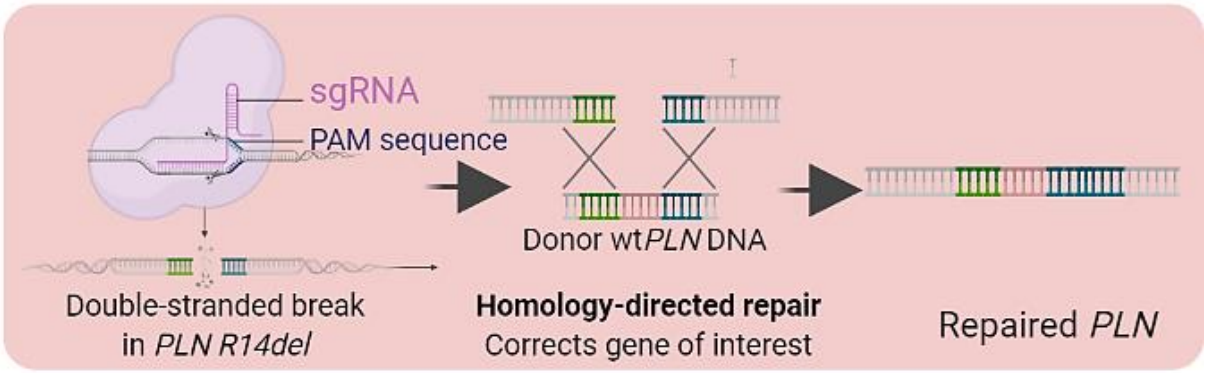

Figure 14: CRISPR/Cas9 method for genome correction of PLN R14del mutation. *The CRISPR-Cas9 enzyme is directed to the mutated PLN gene by sgRNA, which recognises this specific sequence. This recognition is only possible if the sequence is followed by a PAM. When Cas9 binds, a dsDNA break is created, which induces HDR. Due to the presence of a repair template, encoding wtPLN DNA, the mutation is corrected for wtPLN and endogenous PLN R14del is deleted. CRISPR, clustered regularly interspaced short palindromic repeats; Cas9, CRISPR associated protein 9; HDR, homology directed repair; PAM, protospacer adjacent motif; PLN, phospholamban; sgRNA, single-stranded guide RNA; wt, wild-type. Created with BioRender.*

4.3.2.3 siRNA KD R14del

The potential to treat the PLN R14del-induced phenotype with siRNA to knockdown R14del mRNA, might have arisen after investigations by del Monte *et al.* (2002) and Watanabe *et al.* (2004)[108,109]. Del Monte *et al.* discovered that transfection of an adenovirus vector containing antisense of PLN led to improved contraction and relaxation velocities in myocardial cells from human failing hearts[108]. The administration of PLN-antisense inhibited translation of PLN mRNA, and thus production of the protein. The results from this experiment indicated that PLN can be targeted using viral vectors and that this approach may provide therapeutic benefits in human heart failure[108]. Moreover, research of Watanabe *et al.* revealed that cultured neonatal rat cardiac myocytes with decreased SERCA2a protein levels, could be treated with siRNA against PLN. Hereby, endogenous PLN expression was inhibited and Ca^{2+}-uptake affinity by the SR was restored[109]. siRNAs induce gene silencing by binding to PLN mRNA and thereby triggering mRNA degradation, mediated by RNA-induced silencing complex (RISC). This technique has shown more efficient results than the use of antisense RNAs. Combined, these investigations might have broken new ground to investigate the potential of siRNA to knockdown PLN R14del and reveal its effect on the PLN R14del phenotype (Figure 15). These results might open doors towards the actual development of new therapeutics.

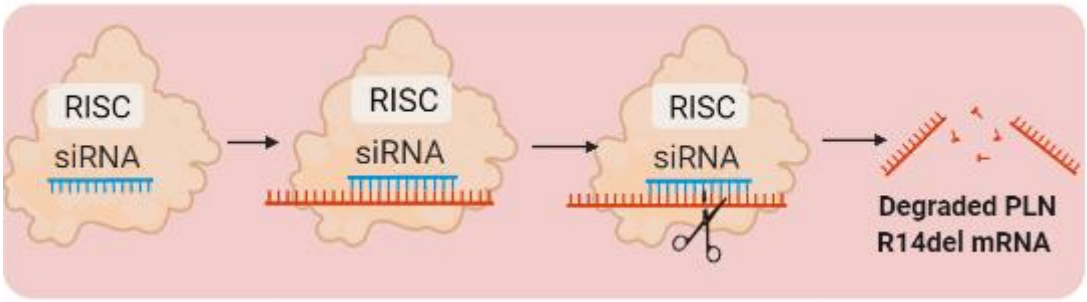

Figure 15: siRNA as a therapeutic approach to KD PLN R14del mRNA. *siRNA is recruited by the RISC complex and binds to complementary mRNA, in this case PLN R14del mRNA. Hereafter, mRNA is cleaved at a specific site and is degraded in the cell. This leads to no translation of the mRNA to the mutated PLN protein. KD, knockdown; mRNA, messenger RNA; PLN, phospholamban; RISC, RNA-Induced silencing complex; siRNA, small interference RNA. Created with BioRender.*

4.3.2.4 ASO

Recent advances in nucleic-acid based therapeutics have elicited high expectations to develop new treatments for various diseases. However, due to the poor binding affinity, specificity, and instability of the nucleic acids, clinical use has been limited[110,111]. Therefore, modified RNA molecules are generated in which a ribose sugar moiety is locked by an oxymethylene bridge that connects the C2' and C4' atoms, leading to less degradation by nucleases and inflammatory effects of the innate immunity[111]. This leads to nucleic acids that have high binding affinity to complementary RNA/DNA and have reduced off-target effects; the Locked nucleic acids (LNAs). A plethora of studies has shown the broad potential of LNA-modified oligonucleotides in antisense-mediated gene-silencing applications *in vitro* and *in vivo* for multiple diseases, including cardiomyopathies[111–113].

A study by Morihara *et al.* (2017) has studied the usefulness of LNA antisense oligonucleotides (LNA-ASOs) *in vivo* as a treatment for heart failure, by targeting PLN[111]. They injected male C57BL/6 mice, subjected to transverse aortic constriction surgery, intravenously with Cy3-labeled LNA-ASO and discovered that this modified RNA could infiltrate into the adult mouse myocardium[111]. Single dose of PLN-targeting LNA-ASO significantly enhanced systolic function and contractility in pressure overload-induced cardiac dysfunction[111]. Although the redistribution of LNA-ASO in the heart is <5% of the total dose, the effective concentration seems to be successful in supressing PLN expression without inducing liver toxicity[111].

These results suggest that PLN-targeting LNA-ASO is a strong candidate to inhibit PLN R14del mRNA in combination with an AAV-based gene delivery approach, to modulate the SERCA2a-PLN axis (Figure 16). AAV-mediated delivery could enhance site-directed delivery, redistribution, and a reduction in side-effects. This method is currently investigated in a murine model in Groningen.

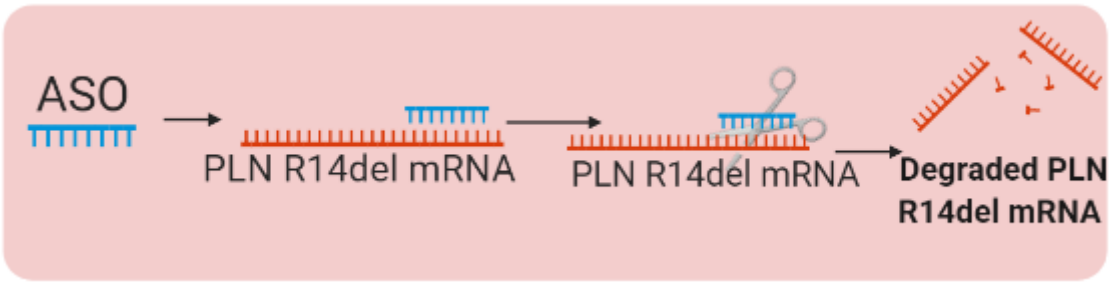

Figure 16: Using LNA-ASO to inhibit PLN R14del mRNA translation. *PLN R14del mRNA translation is inhibited by ASO. ASO hybridised with PLN R14del mRNA and forms an ASO-mRNA heteroduplex. This complex hinders ribosomal subunit binding and thus translation of the mRNA. Additionally, the complex activates RNaseH, leading to degradation of the mRNA. ASO, antisense oligonucleotide; mRNA, messenger RNA; PLN, phospholamban. Created with BioRender.*

Chapter 5: General discussion

5.1 Final remarks on (recombinant) adeno-associated viruses

The aim of this thesis was to discover how AAVs can be altered and be used as recombinant vectors for gene therapy approaches, specifically for PLN R14del patients. It has become clear that AAVs are promising gene delivery vehicles due to their capability to transduce a broad spectrum of proliferating and quiescent cell types, their long-term transgene expression upon once-off delivery, and their low immunogenicity. Although substantial progress has been made in the field of gene therapy, developments in unravelling AAVs are still needed to create viable AAV-strategies for a wide range of human disorders, including AAV-mediated gene therapy. This will guide the generation of rAAVs which are modified to become non-immunogenic, more specific, and efficient by interfering with the AAV transgenic genome, capsid, and steps in the AAV life cycle. The biggest remaining question of generating efficient gene transfer vehicles from AAVs, is how to improve tissue tropism and how to overcome rate-limiting steps upon transduction. These will be discussed in this chapter, along with some suggestions for future directions.

It has become clear that AAVs are altered by excision of the entire *Rep* and *Cap* genes and insertion of a transgene cassette between the ITRs, to generate recombinant AAVs. However, these changes of the AAV genome alone do not determine the transduction efficiency or tissue tropism of the recombinant vectors. In order to generate cardiac specific rAAVs, with high efficient cardiac transduction and minimal undesirable gene delivery to other organs, the AAV capsid should be carefully considered. Chapter 2 highlighted the variation in capsid morphology between AAV subtypes and its influence on tissue tropism and transduction efficiency. One major challenge of gene therapy is that AAVs are not specific enough and are absorbed into cells that are not supposed to be targeted, decreasing transduction efficiency at the intended target side and causing side-effects. Choosing the optimal AAV capsid does not only determine the vectors capability to attach to the target cell, but it also influences accessibility to co-receptors which in turn determine the endocytic pathway. As discussed in Chapter 3, the most productive pathway is the GLIC/CEEC pathway which will lead to an efficient trafficking route along the syntaxin 5 network towards the TGN and the nucleus. By generating specific AAV capsids, these routes that lead to successful and specific transduction can be influenced. Moreover, the AAV capsid additionally influences endosomal escape essential for transgene delivery.

One potential upcoming avenue to influence AAV capsids for specific AAV variants, is through the guided mutation of the capsid to (i) alter their binding to known receptors, or to (ii) gain their dependence on host factors for transduction. A new promising approach by Harvard's Wyss Institute for Biologically Inspired Engineering has arisen that generates AAV capsids using synthetic biology[114]. This technique leads to the creation of AAV capsids with different or more selective cell type and tissue-targeting abilities, by generating multiple variants of the *Cap* gene via mutations. These efforts are currently leading to the identification of specific combinations of mutations that increase target cell specificity and enhance immune evasion potential of the synthetic AAV serotypes, without compromising capsid stability. This approach should be further investigated for cardiac tropism, as it yields the highest functional diversity of any capsid library thus far and unlocks new serotypes with many potential applications for generating improved viral vectors. Generation of highly cardiac specific capsids will make the actual implementation of AAV-mediated gene therapy for PLN R14del patients more feasible.

Not only the viral attachment and endocytic trafficking are important for the transduction efficiency, there is also evidence that post-endocytic trafficking steps, such as nuclear import, can drastically alter

transduction efficiency. As discussed in Chapter 3, only 17% of the AAV virions that dock to the NPC are actually imported. This phenomenon is most likely caused by complex capsid modifications in the endomembrane system. Evaluation of the efficiency and kinetics of AAV nuclear import and nucleolar mobilisation, as discussed in Chapter 3, is needed to improve or overcome this limitation. rAAV nuclear import efficiency might be enhanced through the engineering of an AAV particle with NLSs that recruit multiple Importin receptors to the import complex. Further investigation to clarify enigmatic steps of AAV capsid processing, endosomal escape, nuclear import, and uncoating is crucial and this information might be translated into rapid and major improvements in (cardiac) gene therapy applications.

Moreover, another consideration of rAAVs is the design, which was discussed in Chapter 4. Generation of a rAAV that carries a ssAAV genome will allow carriage of a bigger genome than a scAAV genome, which can only carry half of the ssAAV genome. However, this latter option will bypass the rate-limiting step of conversion of the genome to a double-stranded form and will lead to quicker expression kinetics and stronger expression levels. Current investigations of reversing the PLN R14del phenotype are focussed on techniques such as, CRISPR-Cas9, siRNA, or ASOs. When applying this point of discussion to PLN R14del patients, all of these transgene expression cassettes are of small sizes that do not exceed the 2.4 kb and therefore the scAAV genome strategy seems to be the most promising and efficient method for this specific disease.

The last point of discussion that will be reviewed, is the AAV production strategy. It is of crucial importance for the development of AAV-mediated gene therapy, that a production strategy capable of producing high quantities of rAAVs is used. For successful application of gene therapy in clinical trials, production and purification processes need to meet quantitative and qualitative demands of regulatory agencies; production strategies need to rise on an industrial scale. Three expression systems have been discussed in Chapter 4 that differ in per cell vector productivity, process robustness, and elimination of process and product-related impurities. Although the baculovirus expression system still needs improvements, this system is currently the most promising method to overcome scale-up limitations. Because this technique uses bioreactor systems to scale-up, it is capable of producing sufficient quantities of AAV vectors. This is perfect to initiate preclinical projects in large animal models; a possible future direction for the investigated therapeutic approaches for PLN R14del patients.

5.2 Recombinant adeno-associated viruses as a tool in PLN R14del therapeutic research

Three different potential therapeutic approaches for PLN R14del have been discussed in Chapter 4, which all use AAVs as gene delivery vehicles. The CRISPR-Cas9 method, used to correct the mutated *PLN* gene, will provide new opportunities to study underlying mechanisms of PLN R14del pathogenesis. In addition to its attribution to basic research, this technique also holds enormous potential as a therapeutic. Deploying CRISPR-Cas9 therapeutics directly to the human body, could be of great potential to the treatment of not only PLN R14del diseases, but numerous others. Positive *in vivo* results of the murine PLN R14del model, will highlight AAVs safe and effective delivery of the genome editing reagent to cardiomyocytes. These results will form the proof-of-concept, needed to proceed to human applications. The bridge towards human applications is not inconceivable, as a phase 1/2 clinical trial is currently open for LCA10 patient enrolment (ClinicalTrials.gov Identifier: NCT03872479). This trial employs an AAV-CRISPR delivery directly to the eye, in order to correct a *CEP290* mutation.

The results of this study will evaluate the safety, tolerability, and efficacy of a single dose, paving the way for the use of this technique for PLN R14del as well.

Moreover, a siRNA approach to knockdown the R14del mRNA also has serious therapeutic potential. At this moment, the major target organ of siRNAs remains limited to the liver. Multiple drug candidates for the liver are moving through phase I, II, and III clinical trials[115]. These experiments have yielded impressive safety and efficacy controls and have even let to the approval of a siRNA drug for the treatment of a neurodegenerative disease[115]. Furthermore, an experiment by Sugo *et al.* (2016) that conjugated siRNAs with anti-CD71 Fab' fragment has shown durable gene-silencing results in the heart and skeletal muscle for several months after administration in mice with peripheral artery disease[116]. Therefore, it is not unconceivable that developments in this field will lead to viable and efficient carriers towards the heart. Advancements and considerable efforts are needed, but the first stepping stones to use this technique for PLN R14del have been made. This brings a new era of hope for PLN R14del patients for treatment options with considerable probabilities of halting the disease.

The last investigated therapeutic approach using rAAVs, is the use of ASOs to inhibit PLN R14del translation. This field is also an emerging area of drug development, targeting the disease source at the RNA level. ASOs, together with siRNAs, offer promising alternatives to therapies that target downstream processes. Moreover, ASOs are not new to the market as several antisense therapies are FDA-approved and many drug candidates are in clinical trials. Notably, a potential drug candidate for hypertriglyceridemia, a cardiovascular disease, is currently in a phase II clinical study (ClinicalTrials.gov Identifier: NCT03385239). Positive outcomes of PLN R14del research will form a proof-of-concept which might be rapidly translated to personalised medicine for clinical use. This fact track might seem feasible, due to the fact that ASO-based drugs have gathered momentum since the FDA and EMA approvals for clinical applications. Therefore, positive results might improve PLN R14del patients' lives by halting the disease progression.

Contrary to the DNA/RNA approaches, DWORF overexpression might also be beneficial. This protein is discussed in the practical report. The DWORF protein, with its small size, can be easily packaged in AAV vectors and can be rapidly translated within the cell. Its small size might make delivery even easier than the DNA/RNA constructs and its effect on wtPLN and heart failure has proven its potential for PLN R14del. DWORF overexpression might be capable of displacing PLN R14del from the SERCA2a pump hereby enhancing SERCA2a activity. Restoration or amelioration of SERCA2a activity could improve cardiac cycling and might lead to mitigation of ventricular arrhythmias, contractile dysfunction, heart failure, and sudden cardiac death.

All of these therapeutics hold serious potential as a therapeutic for PLN R14del and at least one of them will meet the criteria needed to proceed with further steps. However, additional developments, trials and long-term clinical experience are still needed to stratify the effect of the different therapeutics and to determine the best treatment strategy. There is still a long way to go and many advances to be made, but the cure for PLN R14del patients is getting one step closer each day. On top of this, with the development in therapeutics for PLN R14del, bridges will be built towards the utility of these strategies for a plethora of other diseases.

Chapter 6: Practical report - Cloning DWORF into expression plasmids for PLN R14del human cardiomyocyte transfection

6.1 Introduction

A new promising approach to tackle PLN R14del induced heart failure has arisen, after the recent discovery of a micro peptide regulator of SERCA2a, called DWORF[12]. This peptide is expressed almost exclusively in cardiac ventricle muscle and has coronary vasoconstrictor functions. Additionally, it was found that this peptide acts as a potent stimulator of SERCA2a activity by competing with PLN to occupy the putative SERCA2a binding site. This results in higher Ca^{2+} storage levels and enhanced contractility[12]. Interestingly, DWORF is capable of activating SERCA2a in the presence as well as in the absence of PLN, due to its high affinity for SERCA2a. Moreover, experiments in mice by Nelson *et al.* (2016) led to the discovery that overexpression of DWORF results in even higher Ca^{2+} transient amplitudes and SR Ca^{2+} loads in cardiomyocytes than seen with wildtype PLN[117]. Additionally, Makarewich *et al.* (2018) demonstrated that super-inhibition of SERCA2a, caused by wildtype PLN overexpression, could be relieved by DWORF overexpression in PLN/DWORF transgenic mice[12]. This resulted in higher Ca^{2+} storage in the SR and enhanced cardiomyocyte contractility[12,117]. Furthermore, Makarewich *et al.* (2018) used a DCM mouse model with a genetic deletion of the muscle-specific LIM domain protein (MLP) to investigate the therapeutic potential of DWORF for HF[12]. DWORF overexpression in this mouse model restored cardiac functioning and prevented pathological remodelling and Ca^{2+} dysregulation, which is normally exhibited by these MLP knock-out (KO) mice[12]. The prevention of the DCM phenotype, seen in MLP KO mice, by DWORF overexpression stresses the clinical potential of DWORF overexpression as a promising therapeutic for HF and makes it an attractive candidate for AAV gene therapy studies[12]. In 2020, this group explored this therapeutic potential, using an AAV9 approach with a cardiac troponin-T promotor in MLP KO mice and in a myocardial infarction mouse model of HF[118]. DWORF gene therapy resulted, in both models, in enhanced ventricular function and reduced cardiac dilation[118].

The outcomes of Makarewich *et al.*'s research highlights the promise of DWORF gene therapy as a novel HF therapeutic[12,118]. Interestingly, the overexpression of DWORF has never been researched in relation to PLN R14del patients. However, this disease is also characterised by increased diastolic intracellular calcium concentrations and depressed SR Ca^{2+}-uptake. Therefore, overexpression of DWORF in these PLN R14del cardiomyocytes might be beneficial to disease prognosis and might even be therapeutic (Figure 17).

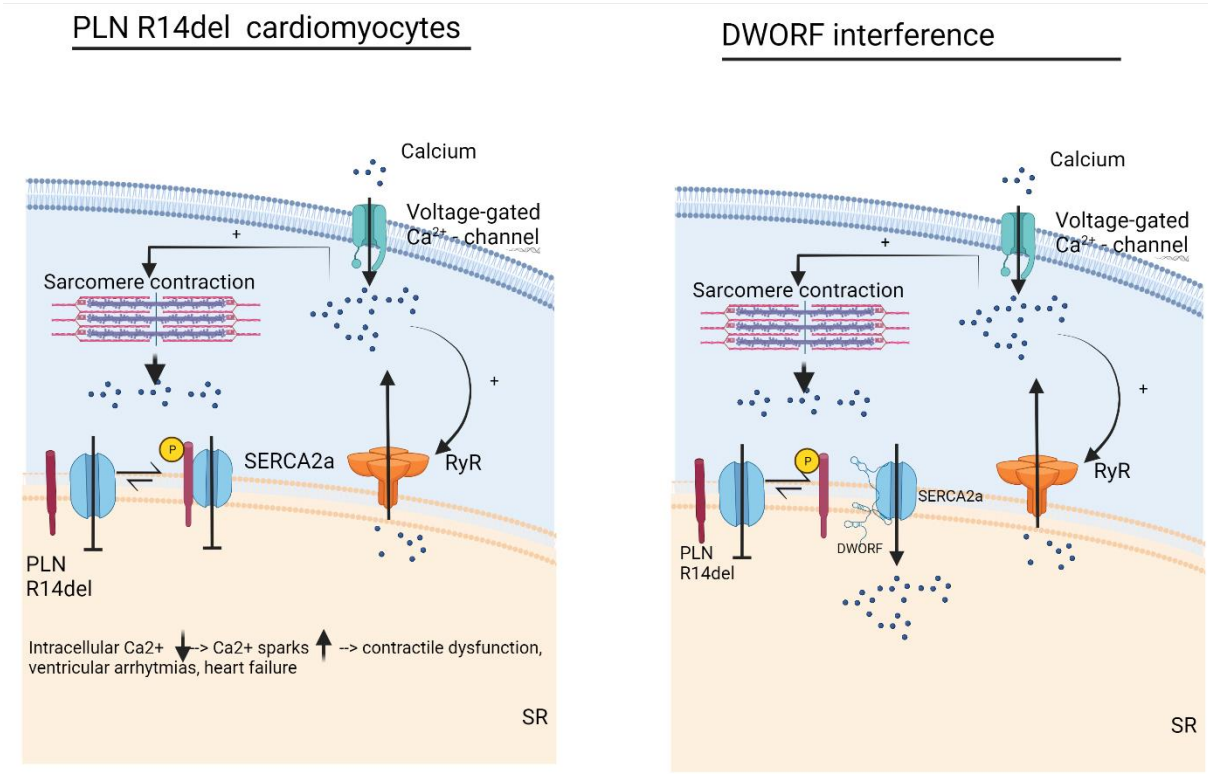

Figure 17: ***Mechanism of Ca^{2+}- cycling in PLN R14del cardiomyocytes with and without DWORF expression.*** *(Left) A deleterious mutation of Arginine 14 codon in the PLN gene (R14del) results in a PLN protein incapable of abolishing the inhibitory interaction with SERCA2a upon phosphorylation. This results in constitutive inhibition of SERCA2a and no uptake of Ca^{2+} in the SR. The Ca^{2+} homeostasis is dysregulated, resulting in increased intracellular Ca^{2+}, decreased Ca^{2+} sparks during contraction, contractile dysfunction, ventricular arrhythmias, and heart failure. (Right) Hypothesis of the effect of DWORF on the PLN R14del-induced super-inhibition of SERCA2a. It is hypothesised that DWORF is capable of displacing PLN R14del from the SERCA2a pump, hereby increasing SERCA2a affinity and restoration of Ca^{2+}-cycling. Hereby, the PLN R14del phenotype might be reversed. Ca^{2+}, calcium; DWORF, dwarf open reading frame; PLN, phospholamban; RyRs, ryanodine receptors; SERCA2a, sarco(endo)plasmic reticulum calcium ATPase 2a; SR, sarcoplasmic reticulum. Created with BioRender.*

Mechanistic understanding of how DWORF could neutralise PLN R14del induced super-inhibition, could lead to disease-specific therapeutics. Therefore, in this study, it is investigated whether human DWORF overexpression could prevent PLN R14del-induced super-inhibition of SERCA2a to improve the function of mutated hiPSC-CMs and human engineered cardiac tissues (hECTs)[119]. Due to the fact that there are major discrepancies in the PLN R14del phenotypes between humans and mice, hiPSCs-CMs and hECTs are favoured to extend this study to human models[119]. These cell mimic the abnormal distribution and perinuclear localisation of PLN protein, similar to the myocardium of PLN R14del patients[119,120]. The CMs and hECTs additionally exhibit the impaired Ca^{2+} handling, twitch force generation and contractile kinetics, increased diastolic Ca^{2+}, and an arrhythmogenic phenotype[119]. This practical report focusses on the creation of three vector constructs to overexpress DWORF, DWORF-GFP, and DWORF-HA in human (PLN R14del) cardiomyocytes.

6.2 Methods

6.2.1 Obtaining smaller vector constructs from a GFP-HA-DWORF vector

A GFP-HA-DWORF_inPF45 pcDNA3-1(+) Puro 6007 bp vector construct (PF773) was designed and sequenced using Macrogen (Figure 18). The exact sequence of this vector can be found in supplementary table 1. Next to this vector construct, multiple smaller linear constructs, containing either the DWORF-HA (PF774), DWORF-GFP (PF775) or only DWORF (PF776) DNA are established using polymerase chain reaction (PCR). The DWORF-HA vector allows detection of DWORF in hiPSC-CMs via western blotting (WB) and the DWORF-GFP vector allows detection of DWORF in hiPSC-CMs via WB and/or fluorescence. Additionally, a DWORF vector was built to determine whether addition of an HA-tag or GFP protein disrupts the function of the micro peptide DWORF.

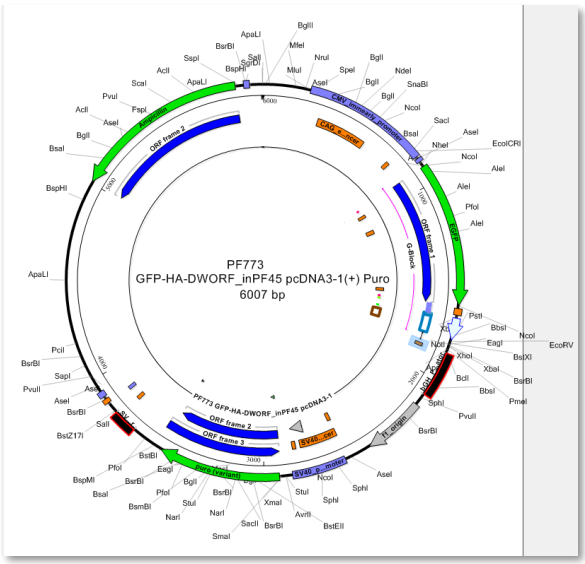

Figure 18: Vector construct GFP-HA-DWORF*. This vector consists of 6007 bp and contains DNA sequences for DWORF, GFP and a HA-tag. Included in the vector construct are also an ampicillin resistance gene, an SV40, and a CMV promotor. Enzymatic restriction sites are depicted around the vector.*

Therefore, the ordered GFP-HA-DWORF vector (340 ng/µl, Macrogen) was diluted by adding 1 µl of vector to 69 µl of TE (10mM Tris/1mM EDTA, pH 8.0), to acquire a concentration of 5 ng/µl. A PCR mix was prepared for 6 reactions in total, as every vector construct sample was run twice. The content for each sample consisted of: 10 µl Buffer GC (5x), 1.5 µl dNTPs, 28 µl Milli-Q, and 0.5 µl Phusion Taq 0530. To each vector duplicate, additional 1.5 µl $MgCl_2$ was added and 3 µl of FV and RV primers were added to all PCR tubes. The primers needed to generate the DWORF-HA construct were F590 (FW) and P591 (RV). To obtain DWORF-GFP: F592 (FW) and F593 (RV) and for DWORF: F592 (FW) and F591 (RV). The exact primer sequence needed for each construct can be found in Appendix 1.1. Hereafter, 44 µl PCR mix and 2 µl GFP-HA-DWORF vector was transferred to each PCR tube and the PCR reaction was run in a Veriti 96 well Thermal Cycler (Applied Biosystems). The following program was used: 1x 120 sec. 98 ºC, 6x (20 sec. 98 ºC, 20 sec. 66 ºC, 2:30 min. 72 ºC), 22x (20 sec. 98 ºC, 15 sec. 63 ºC, 2:30 min. 72 ºC) and increased ''5 after 15 cycles, 15 sec. 72 ºC.

Subsequently, agarose gel electrophoresis was performed to analyse which condition provided the best results to create the linear vector constructs. 80 mL of pre-melted 1% agarose was mixed with 1:10.000 (8 µl) of Midori green dye (LOT: Ba20131205, Nibbon Genetics Europe GmbH), poured in a tray and let to solidify, whereafter the gel was covered with 1x TAE buffer. 4.0 µl loading buffer and 0.5 µl DNP1 enzyme (LOT: 031212, BioLabs) was pipetted into the PCR reaction tubes and 4 µl of each vector construct sample was loaded on gel.

6.2.2 Isolation of successful PCR products

After analysis of the agarose gel, successful PCR products have been isolated. Therefore, 5 g of agarose was added to 500 ml 1x TAE buffer and the mixture was heated in a microwave at 850 W until all of the agarose was dissolved. Next, 20 ml 1x TAE buffer was mixed with 60 mL of the created 1% agarose and 1:10.000 (8 µl) of Midori green dye (LOT: Ba20131205, Nibbon Genetics Europe GmbH) was added. The mixture was poured and let to solidify in a tray, whereafter the gel was covered with 1x TAE buffer.

4.0 µl of loading buffer was pipetted into the PCR reaction tubes and 3x 10 µl of each vector construct sample was loaded onto the gel. Analysis of the gel was performed using a Dark Reader transilluminator (Clare Chemical Research, US) to prevent occurrence of DNA damage in our PCR products. The PCR products were cut out from the gel and were placed into 1.5 mL tubes. The DNA from the agarose gel band was purified, using an Illustra GFX PCR DNA and Gel band purification kit (LOT: 9647922). This step was performed according to the instruction manual of the manufacturer.

6.2.3 Circularisation of the linear vector constructs

The linear constructs needed to be circularised, to regain functional vector constructs again. Therefore, 8.5 µl purified linear vector construct sample, 1 µl ligase buffer (LOT: 1081408, BioLabs) and 0.5 µl T4 polynucleotide kinase (10,000U/mL, LOT: 0880109, BioLabs) was added to a 1.5 ml tube. A mix was prepared, containing 1.5 µl Ligase buffer (LOT: 1081408, BioLabs), 12 µl Milli-Q and 1.5 µl T4 DNA ligase (40,000 cohesive end units/ml, LOT: 1071209, BioLabs). 4 µl of the mix was added to each 1.5 ml tube and the samples were put into the Thermomixer Comfort (Eppendorf) at 16ºC until the next day, to allow for sufficient circularisation to occur.

6.2.4 Transformation of *E.coli* top10 strain with vector constructs

In order to transform an *E.coli* top10 strain with our vector constructs, Luria-Bertani (LB) agar plates were prepared. First, LB Broth was prepared by adding 50 g of Difco LB Broth (miller Luria-Bertani, LOT: 520513) powder to two litres of purified water. This was mixed thoroughly until all of the powder was dissolved. Second, two 500 ml bottles were filled with 6 grams of Bacto Agar (LOT: 4267718) powder and filled up to 400 ml with the prepared LB Broth mixture. The bottles were put into the Tuttnauer Autoclave - Steam sterilizer 3870 ELV. (SER. No 9701029). Hereafter, 1:666 (600 µl) ampicillin (LOT: 130785, Serva) was added to the bottles and the mixture was poured into several Petri dishes and let to solidify.

Transformation was induced by adding 4.5 µl of the circularised vector construct products to 50 µl competent *E.coli* top10 strain cells. The mixture was put on ice for 20 minutes. Next, the mixture was placed in a water bath at 37ºC for 2,5 minutes, and again on ice for 2 minutes. The S.O.C medium (2% tryptone, 0.5% yeast extract, 10mM NaCl, 2.5 mM KCl, 10mM $MgCl_2$, 10 mM $MgSO_4$, and 20 mM glucose, ThermoFisher scientific) was added to each mixture to obtain maximal transformation efficiency, the mixtures were put in the water bath at 37ºC for 30 min. Thereafter, the mixtures were centrifuged to create a bacteria pellet. Lastly, the supernatant was discarded and the pellet was plated onto the Petri dishes and put into the incubator at 37ºC overnight.

6.2.5 Colony PCR

A colony PCR was performed to indicate which colonies had taken up the vector construct successfully. PCR strips were prepared with 100 µl Milli-Q and LB agar plates were prepared with five marks for the generated DWORF-HA single colonies, seven marks for DWORF-GFP single colonies and four marks for DWORF single colonies. From every plate, single colonies were picked and small streaks were made on the fresh bacterial plate. The tip was put into the corresponding tube of the PCR strips. The PCR tubes were boiled for 5 minutes at 95ºC in the Veriti 96 well Thermal Cycler (Applied Biosystems). A PCR mix was prepared separately for each primer combination: F165/14 and F165/NP0520. The exact primer sequence for each construct can be found in Appendix 1.2. The PCR mix for primers F165/14 consisted for each reaction of: 1.5 µl Buffer GC (5x), 0.35 µl F165, 0.35 µl F14, 0.2 µl dNTPs, 0.1 µl Taq (LOT: 0141309, BioLabs), and 7.5 µl Milli-Q. The PCR mix for primers F165/NP0520 consisted for each reaction of: 1.5 µl Buffer GC (5x), 0.35 µl F165, 0.70 µl NP0520, 0.2 µl dNTPs, 0.1 µl Taq (LOT: 0141309,

BioLabs), and 7.15 µl Milli-Q. 5 µl of vector construct template was added to each PCR tube and the PCR program was run on a Veriti 96 well Thermal Cycler (Applied Biosystems). For primers F165/14, the PCR program was as follows: 1x 60 sec. 95 ºC, 35x (15 sec. 95 ºC, 15 sec. 54 ºC, 30 sec. 72 ºC), 1x 1 minute 72 ºC and for primers F165/NP520: 1x 60 sec. 95 ºC, 35x (15 sec. 95 ºC, 15 sec. 60 ºC, 30 sec. 72 ºC), 1x 1 minute 72 ºC. Hereafter, 80 mL of 1% agarose was mixed with 1:10.000 (8 µl) of Midori green dye (LOT: Ba20131205, Nibbon Genetics Europe GmbH), poured, and let to solidify in a tray whereafter the gel was covered with 1x TAE buffer. 4.0 µl of loading buffer was pipetted into the PCR reaction tubes and 11 µl of each vector colony sample was loaded on the gel. The gel was analysed to indicate which colonies had taken up the vector construct and had to be transferred to liquid medium. The transfer was induced by adding 1:1000 (350 µl) ampicillin (LOT: 130785) to 350 ml LB medium and by adding 6 ml of this mixture to 10x 50 ml tubes. The tubes were labelled with the corresponding successful colonies. A small streak was made through the single colonies on the Petri dishes labelled with rows and the bacteria were transferred into the 50ml tubes. Hereafter, the tubes were put into the shaking incubator at 37ºC.

6.2.6 mini Plasmid DNA purification

The vector constructs from the successful colonies needed to be purified from the bacteria, using Nucleospin Plasmid Easy Pure, Plasmid DNA purification kit (LOT: 1703/001, Macherey-Nagel). This was performed according to the instruction manual of the manufacturer.

6.2.7 Sanger Sequencing

The purified vector constructs needed to be prepared for sequencing, to check if mutations had occurred. In order to do so, 1.5 µl of the vector construct templates were poured onto a Nanodrop spectrometer to determine the Nucleic Acid concentration via absorption. Nine tubes were labelled for the correct purified colony vector construct and sequencing mixture was added. This mixture contained for each sequencing reaction 2.5 µl F165 primer and the vector construct was diluted to an input of 600µg (60 ug/µl), using Milli-Q. The colonies were named vector construct#number of plated colonies. Concentrations were; 459.6 ng/µl (DWORF-HA#13), 464.4 ng/µl (DWORF-HA#14), 495.9 ng/µl (DWORF-HA#15), 495.8 ng/µl (DWORF-GFP#13), 526.7 ng/µl (DWORF-GFP#14), 523.6 ng/µl (DWORF-GFP#15), 412 ng/µl (DWORF#13), 450.7 ng/µl (DWORF#15), and 393.3 ng/µl (DWORF#16).

Sequencing labels were attached to the tubes and they were sent to Macrogen sequencing lab for further analysis. Sequencing results were checked for either double peaks, indicating point mutations, or rows of double peaks, indicating a frameshift due to insertions or deletions using Chromas Lite software. Raw data can be found in supplementary table 7.

6.2.8 Restriction enzymes

Additional testing was performed to check the validity of the vector construct, using restriction enzymes NcoI and XbaI. The PCR tubes were labelled for each purified colony vector construct and for the used restriction enzyme. To a 1.5 ml tube for NcoI restriction, 11 µl NEB_4* (LOT: 10013536), 2.2 µl NcoI (LOT: 0701101) and 74.8 µl Milli-Q was added. To a 1.5ml tubes for XbaI restriction, 11 µl NEB_4*(LOT: 10013536), 2.2 µl XbaI (LOT: 0021005) and 74.8 µl Milli-Q was added. 1 µl of template and 8 µl of the prepared restriction mixture was added to PCR tubes. The mixture was put in a water bath at 37 ºC for 1 hour.

Hereafter, 80 mL of 1% agarose was mixed with 1:10.000 (8 µl) of Midori green dye (LOT: Ba20131205, Nibbon Genetics Europe GmbH), poured, and let to solidify in a tray, whereafter the gel was covered

with 1x TAE buffer. 4.0 µl of loading buffer was pipetted into the PCR reaction tubes and 12 µl of each purified colony vector sample was loaded on gel. The gel was analysed for correct cleavage of the restriction enzymes into the vector construct, using a ChemiDoc XRS+ Molecular Imager (Serial #13090547, BioRad). Expected cleavage sites for each construct can be found in the Appendix 1.3

6.2.9 Colonies containing a correct vector construct were subsequently transferred to liquid medium

After deciding which colonies contained a correct vector construct, they had to be transferred to liquid medium. Transfer was induced by adding 2.5 ml LB medium to 10x 14 ml tubes. A small streak was made through the single colonies on the Petri dishes labelled with rows and the bacteria were transferred into the 14 ml tubes. Hereafter, the tubes were put into the shaking incubator at 37 ºC. The next day, 1:750 (160 µl) ampicillin (LOT: 130785) was added to 4 previously made bottles, containing 120 ml LB Broth. 1 ml of the inoculated liquid medium was transferred to these bottles and the bottles were put back into the shaking incubator at 37ºC overnight.

6.2.10 midi Plasmid purification

The correctly sequenced vector constructs from the colonies needed to be purified from the bacteria in the LB Broth bottles. Therefore, the plasmid DNA purification Nucleobond Xtra Midi kit (LOT: 1501/005, REF: 740414.50, BIOKÉ) was used. The midi purification was performed according to the instruction manual of the manufacturer, with a deviation in the amount of added Isopropanol. This amount was 3.7 ml instead of 3.5 ml. Hereafter, the purified vector constructs were left in the Thermomixer Comfort (Eppendorf) at 16ºC until the next day. Then the concentration of the vector constructs was measured, using the Nanodrop spectrometer and constructs DWORF-HA-GFP, DWORF-HA and DWORF-GFP were brought to a concentration of 1ng/ µl. Construct DWORF-GFP was brought to a concentration of 0.5 ng/ µl using TE (10mM Tris/1mM EDTA, pH 8.0).

6.2.11 Restriction enzymes

The purified vector constructs were checked again for the possible occurrence of mutations, using restriction enzymes NcoI and XbaI. PCR tubes were labelled for each vector construct and for the used restriction enzyme. To an 1.5 ml tube for NcoI restriction, 4 µl NEB_4*(LOT: 10013536), 1 µl NcoI (LOT: 0701101) and 31.2 µl Milli-Q was added. To an 1.5 ml tubes for XbaI restriction, 4 µl NEB_4*(LOT: 10013536), 1 µl XbaI (LOT: 0021005) and 31.2 µl Milli-Q was added. 1 µl template was added to tubes and 9 µl of the prepared restriction mixture. The mixture was put in the water bath at 37ºC for 1 hour.

Hereafter, 35mL of 1% agarose was mixed with 1:10.000 (3.5 µl) Midori green dye (LOT: Ba20131205, Nibbon Genetics Europe GmbH) poured, and let to solidify in a tray, whereafter the gel was covered with 1x TAE buffer. 4.0 µl of loading buffer was pipetted into the PCR reaction tubes and 12 µl of each vector sample was loaded on the gel. The gel was analysed for correct cleavage of the restriction enzymes into the vector construct. Expected cleavage sites for each construct can be found in the Appendix 1.3.

6.3 Results

6.3.1 GFP-HA-DWORF vector is effectively cleaved into three smaller vector constructs

In order to obtain smaller vector constructs from the vector GFP-HA-DWORF, different primer combinations were used in a PCR reaction. The PCR reaction was performed twice under different conditions; the first run was performed under traditional PCR conditions (normal) and the second one

under traditional PCR conditions with additionally added $MgCl_2$ (+$MgCl_2$) to enhance the fidelity of Taq Phusion 0530. Separation of the PCR products from DWORF-HA on a 1% agarose gel (Figure 19A), showed no results in lane Normal due to a gel loading mistake. The gel band in lane +$MgCl_2$ was of the expected size of 5287 bp. The results of the DWORF-GFP products (Figure 19B) show gel bands in both lanes of the expected size of 5947bp. The intensity of the gel band in lane +$MgCl_2$ is higher, which can be attributed to a higher amount of template that ended up in the well. The same applies for the gel bands seen in Figure 19C, which depicts results of amplification of the DWORF constructs. These results are visible for both lanes at the expected height of 5227 bp, with a higher intensity in the lane +$MgCl_2$. Therefore, it was decided to continue with all the PCR products from the +$MgCl_2$ PCR run.

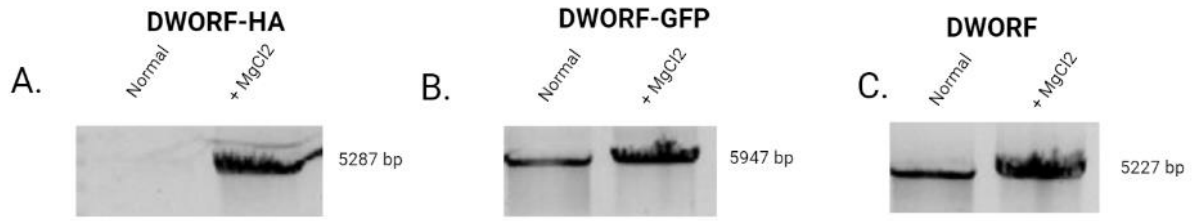

Figure 19: GFP-HA-DWORF vector is effectively cleaved into three smaller vector constructs, using three different primer combinations in a PCR reaction. *GFP-HA-DWORF was amplified in a traditional PCR reaction (lane normal) and in a PCR reaction with additional $MgCl_2$ (lane + $MgCl_2$). 4 µl PCR product was separated on a 1% agarose gel stained with Midori green dye. (A) Gel electrophoresis analysis of linear DWORF-HA vector construct amplification at height of 5287 bp, with no result in lane Normal. (B) Gel electrophoresis analysis of linear DWORF-GFP vector construct amplification at height of 5947 bp for both lanes. (C) Gel electrophoresis analysis of linear DWORF vector construct amplification at height of 5227 bp for both lanes.*

6.3.2 PCR products are successfully isolated from the agarose gel

Next, PCR products from the +$MgCl_2$ PCR run were separated on a 0.8% agarose gel as a preparation step for isolation of these PCR products. The vector constructs all reached the expected height in the gel and were subsequently cut out from the agarose gel (Figure 20). Figure 20A shows the isolated gel band of the DWORF-HA construct and Figure 20B shows the isolated gel band of the DWORF-GFP construct, both with some sample left in the gel on the left. Figure 20C shows the completely isolated gel band of the DWORF construct.

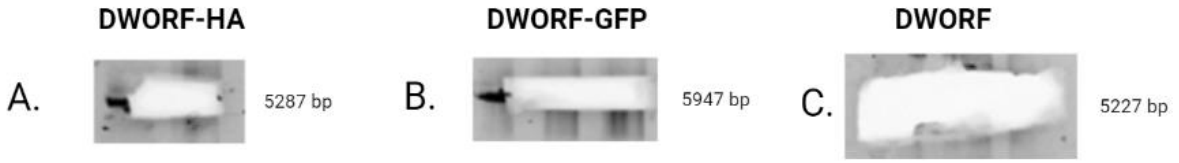

Figure 20: +$MgCl_2$ PCR products are successfully isolated from a 0.8% agarose gel stained with Midori green dye. *Each vector construct sample was loaded and separated on the gel, after which the gel bands were cut out and purified. (A) Gel electrophoresis isolation results from a linear DWORF-HA vector construct that was visible at height of 5287 bp. A part of the gel band is still visible on the left (B) Gel electrophoresis isolation results of linear DWORF-GFP vector construct that was visible at height of 5947 bp. A part of the gel band is still visible on the left. (C) Gel electrophoresis isolation results of linear DWORF vector construct that was visible at height of 5227 bp.*

6.3.3 Colony PCR revealed effective uptake of the DWORF-HA and DWORF-GFP vector constructs in *E.coli* top10 bacteria but an unexpected result for a DWORF colony.

The purified vector constructs were circularised, using a mixture containing ligase and T4 polynucleotide kinase. Hereafter, the vector constructs were transformed into an *E.coli* top10 strain, known for its efficient uptake of plasmids. Colonies were grown overnight on ampicillin LB agar plates, to induce selection of bacteria that had acquired the ampicillin resistance gene that was embedded in the vector construct. Single colonies were picked from the Petri dishes and transferred to traditional PCR mixture, after which a PCR reaction was run. The PCR reaction was run twice, using different primer combinations. The first primer combination let to the amplification of either DWORF-HA,

DWORF-GFP, or DWORF, whereas the second primer combination let to the amplification of GFP. The PCR products were separated on an 1% agarose gel, to indicate which colonies had indeed taken up the vector constructs. Figure 21A shows gel bands for five DWORF-HA colonies (#13-#17), with successful results of the amplification of DWORF-HA (upper row). The gel bands were all of the expected height of 389 bp and indicate successful uptake of the plasmid for all colonies. The bottom row shows no results, which is compatible with the vector that does not contain the DNA for the GFP protein. Figure 21B shows gel bands for seven DWORF-GFP colonies (#13-#19), with successful results for the amplification of DWORF-GFP (upper row). The gel bands were all of the expected height of 1049 bp and indicate successful uptake of the plasmid for all colonies. The bottom row also shows bands of 464bp for every colony, which is compatible with the vector that does contain the DNA for the GFP protein. Figure 21C shows gel bands for four DWORF colonies (#13-#16), with successful results for the amplification of DWORF for most of the colonies (upper row). The gel bands were of the expected height of 1109 bp for colonies #13, #15 and #16. This indicates successful uptake of the plasmid for these colonies. The gel band for #14 is of a lower intensity and the gel band in the bottom row shows a low intensity band as well, whereas this vector does not contain the DNA for a GFP protein. Therefore, DWORF#14 is declared unusable.

Three colonies were picked from every vector construct, to continue with. As all the results were correct for vector constructs DWORF-HA and DWORF-GFP, it was decided to continue with colonies #13-#15. For vector construct DWORF, colonies #13 and #15-#16 were chosen.

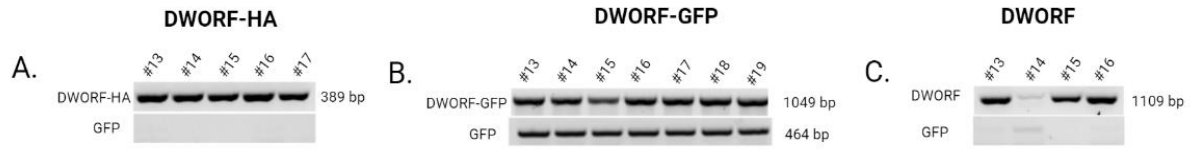

Figure 21: Colony PCR revealed effective uptake of the DWORF-HA and DWORF-GFP vector constructs in E.coli top10 bacteria but an unexpected result for a DWORF colony. *The bacteria were grown on ampicillin LB agar plates, to induce selection between bacteria that did not take up the plasmid and bacteria that did and thereby acquired an ampicillin resistance gene. Colonies were picked from the Petri dishes and added to traditional PCR mixture, after which a PCR reaction was run, using two different primer combinations. The PCR products were separated on a 1% agarose gel, to indicate which colonies had taken up the vector constructs. The gel electrophoresis results are depicted in two rows. The upper row shows amplification of either DWORF-HA, DWORF-GFP, or DWORF and the bottom row shows amplification of GFP. (A) Gel electrophoresis analysis of DWORF-HA colonies, with DWORF-HA results at height of 389 bp for each colony, with no results in the row of GFP. (B) Gel electrophoresis analysis of DWORF-GFP colonies, with DWORF-GFP results at height of 1049 bp for each colony, with results in the row of GFP at height of 464 bp. (C) Gel electrophoresis analysis of DWORF colonies, with DWORF results at height of 389 bp for colonies #13, #15, and #16. Colony#14 shows a lower intensity and results in the row of GFP, whereas the other colonies do not.*

6.3.4 XbaI and NcoI restriction leads to correct cleavage of the DWORF and DWORF-GFP vector, but reveals a mutated colony for DWORF-HA

The vector constructs were purified from the selected *E.coli* top10 strain colonies and were checked for the occurrence of any mutations and for the presence of chromosomal DNA. Therefore, digestion of the purified vectors with NcoI and XbaI was performed. The vector constructs contain restriction sides for both of these enzymes at several locations throughout the vector sequence. The restriction sides for NcoI were predominantly found in the primer binding sites for the creation of the smaller vector constructs from GFP-HA-DWORF. The cleavage products of these enzymes indicate if the constructions were formed correctly and the size of these products was known beforehand and can be found in Appendix 1.3. The purified vector constructs are shown in Figure 22 and depict the cleavage products of NcoI (left) and XbaI (right). A light band is visible for almost every figure just underneath the biggest cleavage product, indicating coiled coil formation of the vector constructs. Restriction

enzymes have difficulty with cleaving these coiled coils. The DWORF-HA vector (Figure 22A) shows correct cleavage by NcoI of the purified vector from colonies #13 and #15, but not for #14. For this colony, the second NcoI cleavage product has a bigger height than expected and the third cleavage product of 295 bp is not produced at all. However, the cleavage products of XbaI are as expected for every colony. A light band is also visible just underneath the biggest cleavage product, indicating coiled coil formation of the vector constructs (structural motifs in the vector leads to coiled helices like strands of a rope). Restriction enzymes have difficulty with cleaving these coiled coils. The smallest cleavage product of XbaI for DWORF-HA is 148 bp and it is only visible in the inverted image on the right. The DWORF-GFP vector (Figure 22B) and DWORF vector (Figure 22C) show correct cleavage by NcoI and XbaI of the purified vector for every colony. The control, depicted in figure 5D, also shows correct cleavage by NcoI and XbaI. The results of this experiment exclude DWORF-HA#14 from any further steps and exclude the presence of chromosomal DNA.

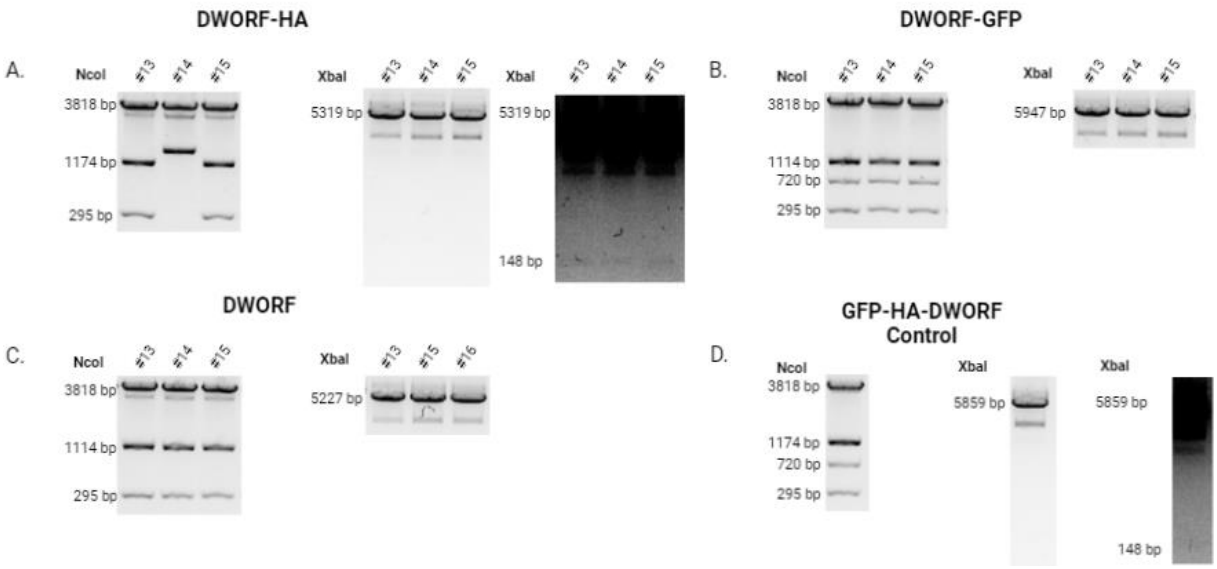

Figure 22: XbaI and NcoI restriction of the mini purified vector constructs leads to correct cleavage of the DWORF and DWORF-GFP vector, but reveals a mutated colony for DWORF-HA*. Vector constructs were purified from the selected colonies and mixed with restriction enzymes NcoI and XbaI. The cleavage sample was separated on a 1% agarose gel stained with Midori green dye. (A) The cleavage products of purified DWORF-HA from three colonies. The cleavage products of NcoI show three bands for colonies #13 and #14 at heights 3818, 1174 and 295 bp. For colony #14, only two bands are visible at respectively 3818 bp and 1500 bp. The cleavage products of XbaI show two bands for every colony at heights 5319 (left XbaI figure) and 148 bp (right XbaI figure). The gels also show light bands just underneath the biggest cleavage product. (B) The cleavage products of purified DWORF-GFP from three colonies. The cleavage products of NcoI show four bands for every colonies at heights 3818, 1114, 720, and 295 bp. The cleavage product of XbaI shows one band for every colony at height 5947 bp. The gels also show light bands just underneath the biggest cleavage product. (C) The cleavage products of purified DWORF from three colonies. The cleavage products of NcoI show three bands for every colonies at heights 3818, 1114, and 295 bp. The cleavage product of XbaI shows one band for every colony at height 5227 bp. The gels also show light bands just underneath the biggest cleavage product. (D) The cleavage products of purified DWORF-GFP-HA from one previously checked colony (control). The cleavage products of NcoI show four bands for the colonies at heights 3818, 1174, 720, and 295 bp. The cleavage product of XbaI shows one band at height 5859 bp (left XbaI figure) and one at height 148 bp (right XbaI figure). The gels also show light bands just underneath the biggest cleavage product.*

6.3.5 Sanger sequencing reveals (non)mutated colonies for each vector construct

The purified vector constructs were additionally checked with Sanger sequencing by Macrogen for any mutations that might have occurred. The results showed the presence of an insertion in DWORF-HA#14, a GFP point mutation in DWORF-GFP#13 and inconclusive results for DWORF#15 and DWORF#16 (Table 4). Raw Sanger sequencing results can be found in Supplementary data 7.

Combining the results from the restriction enzyme digestion and the Sanger sequencing, it was decided to continue with one purified colony vector from each construct, namely DWORF-HA#13, DWORF-GFP#14 and DWORF#13.

Table 4: Sanger sequencing reveals (non)mutated colonies for each vector construct

PURIFIED VECTOR CONSTRUCT	RESULT
DWORF-HA#13	No mutations
DWORF-HA#14	Insertion
DWORF-HA#15	No mutations
DWORF-GFP#13	GFP point mutation
DWORF-GFP#14	No mutations
DWORF-GFP#15	No mutations
DWORF #13	No mutations
DWORF #15	Inconclusive
DWORF #16	Inconclusive

6.3.6 XbaI and NcoI restriction leads to correct cleavage of all vector constructs

The colonies that contained the correct plasmid were expanded in liquid medium overnight and the vector constructs were purified from the *E.coli* top10 strain bacteria again. Hereafter, a restriction enzyme digestion was performed to check for the last time if the vector construct were still correct and did not obtain any mutations. The purified vector constructs are shown in Figure 23 and depict the cleavage products of NcoI (left) and XbaI (right). A light band is visible for almost every figure just underneath the biggest cleavage product, indicating coiled coil formation of the vector constructs. DWORF-HA vector (Figure 23A), DWORF-GFP (Figure 23B), DWORF (Figure 23C), and GFP-HA-DWORF (Figure 23D) all show correct cleavage by NcoI and XbaI. Additionally, the results exclude the presence of chromosomal DNA and thus correctly purified vector constructs.

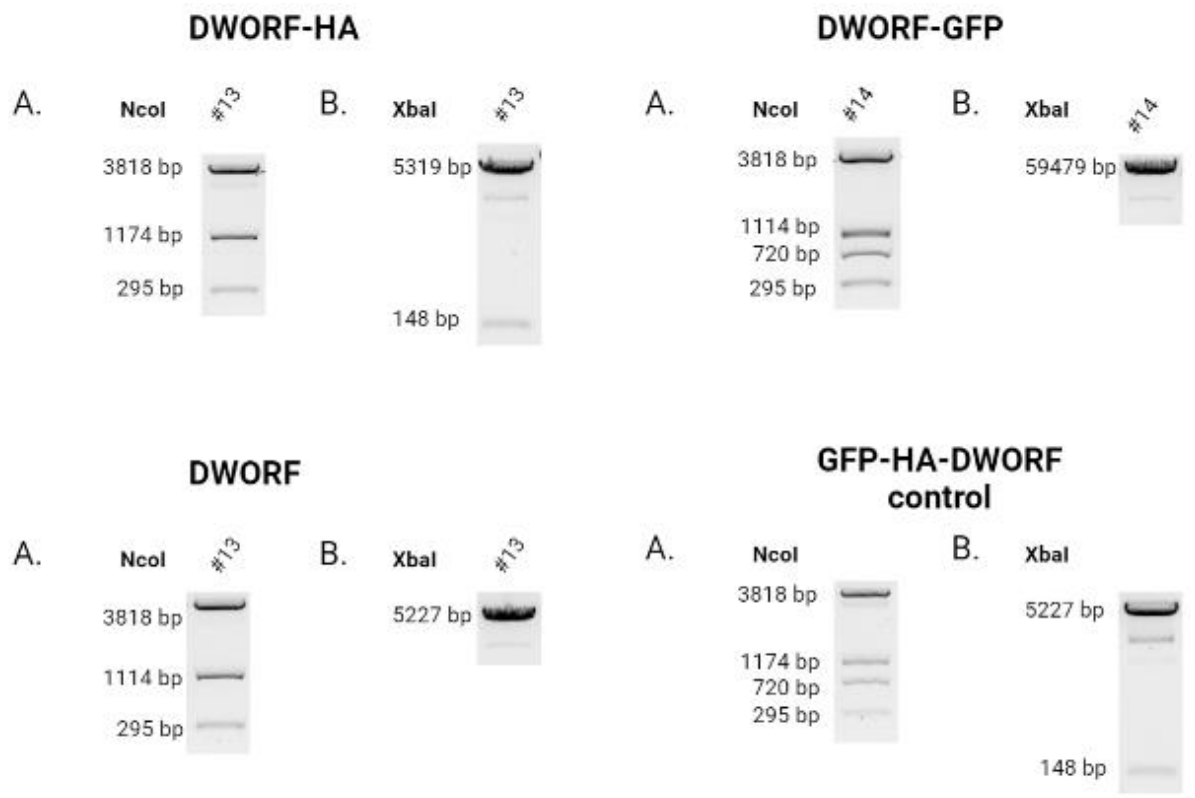

Figure 23: XbaI and NcoI restriction of the midi purified vector constructs leads to correct cleavage of each vector construct. *Vector constructs were purified from the selected colonies and mixed with restriction enzymes NcoI and XbaI. The cleavage sample was separated on a 1% agarose gel stained with Midori green dye. (A) The cleavage products of purified DWORF-HA. The cleavage products of NcoI show three bands at heights 3818, 1174 and 295 bp. The cleavage products of XbaI show two bands at heights 5319 and 148 bp. The gels also show light bands just underneath the biggest cleavage product. (B) The cleavage products of purified DWORF-GFP. The cleavage products of NcoI show four bands at heights 3818, 1114, 720, and 295 bp. The cleavage product of XbaI shows one band at height 5947 bp. The gels also show light bands just underneath the biggest cleavage product. (C) The cleavage products of purified DWORF. The cleavage products of NcoI show three bands at heights 3818, 1114, and 295 bp. The cleavage product of XbaI shows one band at height 5227 bp. (D) The cleavage products of purified DWORF-GFP-HA from one previously checked colony (control). The cleavage products of NcoI show four bands for the colony at heights 3818, 1174, 720, and 295 bp. The cleavage product of XbaI shows one band at height 5859 bp and one at height 148 bp. The gels also show light bands just underneath the biggest cleavage product.*

Discussion

The aim of this research was to generate three smaller vector constructs from the GFP-HA-DWORF vector. It was hypothesised that generation of these smaller constructs would be possible without the occurrence of any mutations and that transcription of these vectors should therefore lead to functional DWORF-GFP, DWORF-HA, and DWORF. Production of DWORF-GFP and DWORF-HA should allow detection of the protein with fluorescence and WB and all three vectors are needed to get a mechanistic understanding of how DWORF could neutralise PLN R14del super-inhibition.

First, two different PCR runs allowed us to generate these three different vector constructs from the GFP-HA-DWORF vector. As expected, both runs generated desired linear vector constructs, except for the normal PCR run that needed to generate the DWORF-HA linear vector construct. This error can be attributed to a gel loading mistake.

Second, competent *E.coli* top10 strain bacteria were transformed with the vector constructs and put on ampicillin LB agar Petri dishes, to induce selection. Bacteria that had taken up the plasmid, should have acquired an ampicillin resistance gene that was embedded in the vector constructs. However, the

Petri dishes showed an overwhelming amount of growth of colonies after 24 hours. This indicated that no selection had occurred and that it would be hard to pick single colonies that had taken up the plasmid, if any. Colony PCR showed no results for any of the colonies that we did pick so we performed another experiment where we plated competent *E.coli* bacteria on Petri dishes with a high amount of ampicillin. The next day, the plate was still filled up with colonies, indicating that the ampicillin we used was not functional. Therefore, the transformation step and subsequently the colony PCR was repeated with a new batch of ampicillin. This colony PCR did show successful results for every picked single colony for every vector construct. From this, we concluded that the linear vector constructs were successfully circularised in a previous step and were indeed taken up by our competent bacteria.

Third, vector constructs were isolated from bacteria and checked for any mutations or presence of chromosomal DNA, using restriction enzymes and Sanger sequencing. The results from the restriction enzyme check were unexpected for the DWORF-HA vector construct, colony #14. There were only two cleavage products, one of which was not of expected height. This indicates that the vector construct lost a NcoI restriction site somewhere during the process. This happened most likely during the generation of the DWORF-HA vector construct via PCR. The amplification of the vector construct must have been unsuccessful, embedding mutations that led to the deletion of a NcoI restriction site. However, other results were impeccable. The Sanger sequencing results revealed the presence of additional mutations in the vector constructs. An insertion was found in the DWORF-HA#14 vector construct, a GFP point mutation in the DWORF-GFP#13 vector construct, and inconclusive Sanger sequencing results appeared for the DWORF#15#16 vector construct.

Lastly, as only one successful colony is needed to purify our vector constructs from, one colony of each vector sample was transferred to liquid medium to expand. Hereafter, the purified vector constructs were checked again using restriction enzymes. This experiment did not reveal any mutations within the plasmids and from that we could conclude that we had successfully generated and purified three vector constructs.

In conclusion, three vector constructs were generated from a GFP-HA-DWORF vector using PCR, transformation, restriction enzymes, and Sanger sequencing techniques. This has led to vector constructs containing the whole DWORF, DWORF-HA, or DWORF-GFP gene. These constructs should be capable of producing functional proteins when transcribed within hiPSCs and hECTs.

Further experiments will provide insight into the capability of DWORF overexpression as a potential PLN R14del treatment. Therefore, the vector constructs will be transfected in hiPSC-CMs and hECTs in next experiments. These models exhibit similarity to the human PLN R14del phenotype; i.e. the abnormal distribution and perinuclear localisation of PLN protein, the exhibition of impaired Ca^{2+} handling, twitch force generation and contractile kinetics, increased diastolic Ca^{2+}, and an arrhythmogenic phenotype.

First, the vector constructs will be transfected in healthy hiPSC-CMs and transduction efficiency will be determined by confirmation of DWORF overexpression using WB. In order to determine the effect of DWORF overexpression on the PLN R14del-induced super-inhibition of SERCA2a to improve human cardiomyocyte function, three types of organoids (PLN R14del, PLN R14del corrected, and wildtype) will be transfected with DWORF-GFP. Hereafter, calcium- and contractility read-outs will be performed to determine whether DWORF overexpression leads to the rescue of the PLN R14del phenotype.

If the results of this experiment indeed prove that DWORF overexpression is capable of reversing the super-inhibition of SERCA2a and improving cardiomyocyte function, future experiments could be interesting that focus on the implementation of these results into the engineering of new AAV delivery techniques. The generation of rAAVs that are able to enter and deliver DWORF expression vectors to hiPSC-CMs and hECTs specifically, could be a huge step in opening doors towards new life-saving therapies for PLN R14del patients.

Appendix

Table 1.1: Primer sequences to obtain vector constructs from GFP-HA-DWORF.

Appendix table 1: Primer sequences needed to generate three different vector constructs from GFP-HA-DWORF vector.

Vector construct	Primer	Sequence	PCR product size
DWORF-HA "GFP-away"	F590 (FW)	GCTTCTAGCTATCCTTATGACGTGC	5287 bp
	F591 (RV)	CATGGTGGCGCTAGCCAG	
DWORF-GFP "HA-away"	F592 (FW)	GCTGAAAAAGCGGGGTCTAC	5947 bp
	F593 (RV)	CATGGACTTGTACAGCTCGTC	
DWORF "HA and GFP -away"	F592 (FW)	GCTGAAAAAGCGGGGTCTAC	5227 bp
	F591 (RV)	CATGGTGGCGCTAGCCAG	

Table 1.2: Primer sequences for colony PCR

Appendix table 2: Primer sequences used for colony PCR of transformed E.coli top10 strain bacteria

Vector construct	Primer	Sequence
F165	FW	CGCAAATGGGCGGTAGGCG
F14	RV	TAGAAGGCACAGTCGA
NP0520	RV	GTCTTGTAGTTGCCGTCGTCGTCCTTG

Appendix table 3: Depiction of the PCR product sizes after a PCR run using different primer combinations.

Primer combination	PCR product size DWORF-HA (bp)	DWORF-GFP (bp)	DWORF (bp)	Control DWORF-HA-GFP (bp)
F165/F14	389	1049	329	1109
F165/NP0520	negative	464	negative	464

Table 1.3: Expected PCR bands after cleavage

Appendix table 3: Depiction of the PCR product sizes after digestion by restriction enzymes NcoI and XbaI.

Restriction enzyme	PCR product size DWORF-HA (bp)	DWORF-GFP (bp)	DWORF (bp)	Control DWORF-HA-GFP (bp)
NcoI	295, 1174, 3818	295, 720, 1114, 3818	295, 1114, 3818	295, 720, 1174, 3818
XbaI	148, 5139	5947	5227	148, 5859

References

1. COVID-19 CORONAVIRUS PANDEMIC. *Worldometers* 1 https://www.worldometers.info/coronavirus/ (2021).
2. Artenstein, A. W. The discovery of viruses: advancing science and medicine by challenging dogma. *International Journal of Infectious Diseases* **16**, e470–e473 (2012).
3. Rosenbaum, A. N., Agre, K. E. & Pereira, N. L. Genetics of dilated cardiomyopathy: practical implications for heart failure management. *Nature Reviews Cardiology* **17**, 286–297 (2020).
4. Andino, L. M. *et al.* AAV-mediated knockdown of phospholamban leads to improved contractility and calcium handling in cardiomyocytes. *Journal of Gene Medicine* **10**, (2008).
5. Bass-Stringer, S. *et al.* Adeno-Associated Virus Gene Therapy: Translational Progress and Future Prospects in the Treatment of Heart Failure. *Heart Lung and Circulation* vol. 27 (2018).
6. Ishikawa, K., Weber, T. & Hajjar, R. J. Human cardiac gene therapy. *Circulation Research* vol. 123 (2018).
7. Hermonat, P. L. & Muzyczka, N. Use of adeno-associated virus as a mammalian DNA cloning vector: Transduction of neomycin resistance into mammalian tissue culture cells. *Proceedings of the National Academy of Sciences of the United States of America* **81**, (1984).
8. Kok, C. Y., Alexander, I., Lisowski, L. & Kizana, E. Directed Evolution of Adeno-Associated Virus Vectors in Human Cardiomyocytes for Cardiac Gene Therapy. *Heart Lung and Circulation* vol. 27 (2018).
9. Feyen, D. A. M. *et al.* The Unfolded Protein Response as a Compensatory Mechanism and Potential Therapeutic Target in PLN R14del Cardiomyopathy. *Circulation* CIRCULATIONAHA.120.049844 (2021) doi:10.1161/CIRCULATIONAHA.120.049844.
10. Haghighi, K. *et al.* A mutation in the human phospholamban gene, deleting arginine 14, results in lethal, hereditary cardiomyopathy. *Proceedings of the National Academy of Sciences* **103**, 1388–1393 (2006).
11. Goedel, A., Grote Beverborg, N., Sahara, M. & Chien, K. R. In search of the next super models. *EMBO Molecular Medicine* **11**, (2019).
12. Makarewich, C. A. *et al.* The DWORF micropeptide enhances contractility and prevents heart failure in a mouse model of dilated cardiomyopathy. *eLife* **7**, (2018).
13. McMichael, A. J. Environmental and social influences on emerging infectious diseases: past, present and future. *Philosophical Transactions of the Royal Society of London. Series B: Biological Sciences* **359**, 1049–1058 (2004).
14. Johnsen, J. Phytopathological Classics number 7. in *Phytopathological classics* 39 (The American Phytopathological Society, 1942).
15. Rybicki, Ed. *A Short History of the Discovery of Viruses*. *Apple iBooks Store* (2015).
16. Bos, L. Beijerinck's work on tobacco mosaic virus: historical context and legacy. *Philosophical transactions of the Royal Society of London. Series B, Biological sciences* **354**, 675–85 (1999).
17. Berche, P. Louis Pasteur, from crystals of life to vaccination. *Clinical microbiology and infection : the official publication of the European Society of Clinical Microbiology and Infectious Diseases* **18 Suppl 5**, 1–6 (2012).
18. van Kammen, A. Beijerinck's contribution to the virus concept--an introduction. *Archives of virology. Supplementum* **15**, 1–8 (1999).
19. Lechevalier, H. Dmitri Iosifovich Ivanovski (1864-1920). *Bacteriological reviews* **36**, 135–45 (1972).
20. Sankaran, N. On the historical significance of Beijerinck and his contagium vivum fluidum for modern virology. *History and philosophy of the life sciences* **40**, 41 (2018).

21. Rossmann, M. G. Structure of viruses: a short history. *Quarterly reviews of biophysics* **46**, 133–80 (2013).
22. Kay, L. E. W.M. Stanley's crystallization of the tobacco mosaic virus, 1930-1940. *Isis 77* 450–472 (1986).
23. Bernal, J. D. & Fankuchen, I. X-RAY AND CRYSTALLOGRAPHIC STUDIES OF PLANT VIRUS PREPARATIONS. *Journal of General Physiology* **25**, 111–146 (1941).
24. Gelderblom, H. R. *Structure and Classification of Viruses*. *Medical Microbiology* (1996).
25. Herrero-Uribe, L. Viruses, definitions and reality. *Revista de biologia tropical* **59**, 993–8 (2011).
26. Lodish H, Berk A, Zipursky SL, et al. Viruses: Structure, Function, and Uses. in *Molecular cell biology* (2000).
27. Simmonds, P. & Aiewsakun, P. Virus classification - where do you draw the line? *Archives of virology* **163**, 2037–2046 (2018).
28. Abergel, C., Legendre, M. & Claverie, J.-M. The rapidly expanding universe of giant viruses: Mimivirus, Pandoravirus, Pithovirus and Mollivirus. *FEMS microbiology reviews* **39**, 779–96 (2015).
29. Patil, S. D., Rhodes, D. G. & Burgess, D. J. DNA-based therapeutics and DNA delivery systems: a comprehensive review. *The AAPS journal* **7**, E61-77 (2005).
30. CROOKE, S. T. An Overview of Progress in Antisense Therapeutics. *Antisense and Nucleic Acid Drug Development* **8**, 115–122 (1998).
31. Patil, S. D., Rhodes, D. G. & Burgess, D. J. DNA-based therapeutics and DNA delivery systems: A comprehensive review. *The AAPS Journal* **7**, E61–E77 (2005).
32. Zacchigna, S., Zentilin, L. & Giacca, M. Adeno-Associated Virus Vectors as Therapeutic and Investigational Tools in the Cardiovascular System. *Circulation Research* **114**, 1827–1846 (2014).
33. Hoggan, M. D., Blacklow, N. R. & Rowe, W. P. Studies of small DNA viruses found in various adenovirus preparations: physical, biological, and immunological characteristics. *Proceedings of the National Academy of Sciences* **55**, 1467–1474 (1966).
34. Atchison, R. W., Casto, B. C. & Hammon, W. McD. Adenovirus-Associated Defective Virus Particles. *Science* **149**, 754–755 (1965).
35. Gonçalves, M. A. F. v. Adeno-associated Virus: From Defective Virus to Effective Vector. *Virology journal* **2:43**,.
36. Balakrishnan, B. & Jayandharan, G. Basic Biology of Adeno-Associated Virus (AAV) Vectors Used in Gene Therapy. *Current Gene Therapy* **14**, 86–100 (2014).
37. Skalka, A. M., Flint, J., Rall, G. F. & Racaniello, V. R. *Principles of Virology, Volume I: Molecular Biology*. *Principles of Virology, Volume I: Molecular Biology* (2015). doi:10.1128/9781555818951.
38. Daya, S. & Berns, K. I. Gene Therapy Using Adeno-Associated Virus Vectors. *Clinical Microbiology Reviews* **21**, 583–593 (2008).
39. Pénzes, J. J. *et al.* Reorganizing the family Parvoviridae: a revised taxonomy independent of the canonical approach based on host association. *Archives of Virology* **165**, 2133–2146 (2020).
40. Mietzsch, M., Pénzes, J. J. & Agbandje-McKenna, M. Twenty-Five Years of Structural Parvovirology. *Viruses* **11**, (2019).
41. Havlik, L. P. *et al.* Coevolution of Adeno-associated Virus Capsid Antigenicity and Tropism through a Structure-Guided Approach. *Journal of virology* **94**, (2020).
42. Meier, A. F., Fraefel, C. & Seyffert, M. The Interplay between Adeno-Associated Virus and Its Helper Viruses. *Viruses* **12**, 662 (2020).

43. Pillay, S. *et al.* Adeno-associated Virus (AAV) Serotypes Have Distinctive Interactions with Domains of the Cellular AAV Receptor. *Journal of virology* **91**, (2017).
44. Schultz, B. R. & Chamberlain, J. S. Recombinant Adeno-associated Virus Transduction and Integration. *Molecular Therapy* **16**, 1189–1199 (2008).
45. Rodríguez-Márquez, E., Meumann, N. & Büning, H. Adeno-associated virus (AAV) capsid engineering in liver-directed gene therapy. *Expert Opinion on Biological Therapy* 1–18 (2020) doi:10.1080/14712598.2021.1865303.
46. Tseng, Y.-S. & Agbandje-McKenna, M. Mapping the AAV Capsid Host Antibody Response toward the Development of Second Generation Gene Delivery Vectors. *Frontiers in Immunology* **5**, (2014).
47. Agbandje-McKenna, M. & Kleinschmidt, J. AAV capsid structure and cell interactions. *Methods in Molecular Biology* vol. 807 (2011).
48. Wörner, T. P. *et al.* Adeno-associated virus capsid assembly is divergent and stochastic. *Nature Communications* **12**, (2021).
49. Venkatakrishnan, B. *et al.* Structure and Dynamics of Adeno-Associated Virus Serotype 1 VP1-Unique N-Terminal Domain and Its Role in Capsid Trafficking. *Journal of Virology* **87**, 4974–4984 (2013).
50. Mayor, H. D., Torikai, K., Melnick, J. L. & Mandel, M. Plus and Minus Single-Stranded DNA Separately Encapsidated in Adeno-Associated Satellite Virions. *Science* **166**, 1280–1282 (1969).
51. Srivastava, A., Lusby, E. W. & Berns, K. I. Nucleotide sequence and organization of the adeno-associated virus 2 genome. *Journal of virology* **45**, 555–64 (1983).
52. Harvey, R. F. *et al.* Trans -acting translational regulatory RNA binding proteins. *Wiley Interdisciplinary Reviews: RNA* **9**, e1465 (2018).
53. Karlin, D. G. Sequence Properties of the MAAP Protein and of the VP1 Capsid Protein of Adeno-Associated Viruses. *Preprints* (2020) doi:10.20944/preprints202002.0234.v1.
54. Wang, D., Tai, P. W. L. & Gao, G. Adeno-associated virus vector as a platform for gene therapy delivery. *Nature Reviews Drug Discovery* **18**, 358–378 (2019).
55. Qin, W. *et al.* Large-scale molecular epidemiological analysis of AAV in a cancer patient population. *Oncogene* **40**, 3060–3071 (2021).
56. Sonntag, F., Schmidt, K. & Kleinschmidt, J. A. A viral assembly factor promotes AAV2 capsid formation in the nucleolus. *Proceedings of the National Academy of Sciences of the United States of America* **107**, 10220–5 (2010).
57. Wu, Z., Asokan, A. & Samulski, R. J. Adeno-associated Virus Serotypes: Vector Toolkit for Human Gene Therapy. *Molecular Therapy* **14**, 316–327 (2006).
58. Choi, V. W., McCarty, D. M. & Samulski, R. J. AAV hybrid serotypes: improved vectors for gene delivery. *Current gene therapy* **5**, 299–310 (2005).
59. Huang, L.-Y., Halder, S. & Agbandje-McKenna, M. Parvovirus glycan interactions. *Current opinion in virology* **7**, 108–18 (2014).
60. Pillay, S. & Carette, J. E. Host determinants of adeno-associated viral vector entry. *Current opinion in virology* **24**, 124–131 (2017).
61. Li, C. & Samulski, R. J. Engineering adeno-associated virus vectors for gene therapy. *Nature Reviews Genetics* vol. 21 (2020).
62. Srivastava, A. In vivo tissue-tropism of adeno-associated viral vectors. *Current Opinion in Virology* **21**, 75–80 (2016).
63. Riyad, J. M. & Weber, T. Intracellular trafficking of adeno-associated virus (AAV) vectors: challenges and future directions. *Gene Therapy* (2021) doi:10.1038/s41434-021-00243-z.

64. Nonnenmacher, M. & Weber, T. Adeno-associated virus 2 infection requires endocytosis through the CLIC/GEEC pathway. *Cell host & microbe* **10**, 563–76 (2011).
65. Nonnenmacher, M. E., Cintrat, J.-C., Gillet, D. & Weber, T. Syntaxin 5-Dependent Retrograde Transport to the trans -Golgi Network Is Required for Adeno-Associated Virus Transduction. *Journal of Virology* **89**, 1673–1687 (2015).
66. Kalia, M. *et al.* Arf6-independent GPI-anchored Protein-enriched Early Endosomal Compartments Fuse with Sorting Endosomes via a Rab5/Phosphatidylinositol-3'-Kinase–dependent Machinery. *Molecular Biology of the Cell* **17**, 3689–3704 (2006).
67. Ding, W., Zhang, L., Yan, Z. & Engelhardt, J. F. Intracellular trafficking of adeno-associated viral vectors. *Gene Therapy* **12**, 873–880 (2005).
68. Kelich, J. M. *et al.* Super-resolution imaging of nuclear import of adeno-associated virus in live cells. *Molecular therapy. Methods & clinical development* **2**, 15047 (2015).
69. Bevington, J. M. *et al.* Adeno-associated virus interactions with B23/Nucleophosmin: identification of sub-nucleolar virion regions. *Virology* **357**, 102–13 (2007).
70. Qiu, J. & Brown, K. E. A 110-kDa nuclear shuttle protein, nucleolin, specifically binds to adeno-associated virus type 2 (AAV-2) capsid. *Virology* **257**, 373–82 (1999).
71. Rossi, A. *et al.* Vector uncoating limits adeno-associated viral vector-mediated transduction of human dendritic cells and vector immunogenicity. *Scientific Reports* **9**, 3631 (2019).
72. McCarty, D. M., Young, S. M. & Samulski, R. J. Integration of Adeno-Associated Virus (AAV) and Recombinant AAV Vectors. *Annual Review of Genetics* **38**, 819–845 (2004).
73. McCarty, D. M. Self-complementary AAV vectors; advances and applications. *Molecular therapy : the journal of the American Society of Gene Therapy* **16**, 1648–56 (2008).
74. Grosse, S. *et al.* Relevance of Assembly-Activating Protein for Adeno-associated Virus Vector Production and Capsid Protein Stability in Mammalian and Insect Cells. *Journal of virology* **91**, (2017).
75. Maurer, A. C. *et al.* The Assembly-Activating Protein Promotes Stability and Interactions between AAV's Viral Proteins to Nucleate Capsid Assembly. *Cell Reports* **23**, 1817–1830 (2018).
76. Earley, L. F. *et al.* Identification and Characterization of Nuclear and Nucleolar Localization Signals in the Adeno-Associated Virus Serotype 2 Assembly-Activating Protein. *Journal of Virology* **89**, 3038–3048 (2015).
77. Naumer, M. *et al.* Properties of the Adeno-Associated Virus Assembly-Activating Protein. *Journal of Virology* **86**, 13038–13048 (2012).
78. Bleker, S., Sonntag, F. & Kleinschmidt, J. A. Mutational Analysis of Narrow Pores at the Fivefold Symmetry Axes of Adeno-Associated Virus Type 2 Capsids Reveals a Dual Role in Genome Packaging and Activation of Phospholipase A2 Activity. *Journal of Virology* **79**, 2528–2540 (2005).
79. King, J. A. DNA helicase-mediated packaging of adeno-associated virus type 2 genomes into preformed capsids. *The EMBO Journal* **20**, 3282–3291 (2001).
80. Nony, P., Chadeuf, G., Tessier, J., Moullier, P. & Salvetti, A. Evidence for Packaging of rep-cap Sequences into Adeno-Associated Virus (AAV) Type 2 Capsids in the Absence of Inverted Terminal Repeats: a Model for Generation of rep-Positive AAV Particles. *Journal of Virology* **77**, 776–781 (2003).
81. Chen, Y. H., Keiser, M. S. & Davidson, B. L. Viral Vectors for Gene Transfer. *Current protocols in mouse biology* vol. 8 (2018).
82. Aponte-Ubillus, J. J. *et al.* Molecular design for recombinant adeno-associated virus (rAAV) vector production. *Applied Microbiology and Biotechnology* vol. 102 (2018).

83. Robert, M. A. *et al.* Manufacturing of recombinant adeno-associated viruses using mammalian expression platforms. *Biotechnology Journal* vol. 12 (2017).
84. Kang, W. *et al.* An efficient rHSV-based complementation system for the production of multiple rAAV vector serotypes. *Gene Therapy* **16**, (2009).
85. Urabe, M., Ding, C. & Kotin, R. M. Insect cells as a factory to produce adeno-associated virus type 2 vectors. *Human Gene Therapy* **13**, (2002).
86. Martino, A. T. *et al.* The genome of self-complementary adeno-associated viral vectors increases Toll-like receptor 9-dependent innate immune responses in the liver. *Blood* **117**, (2011).
87. Galibert, L. *et al.* Origins of truncated supplementary capsid proteins in rAAV8 vectors produced with the baculovirus system. *PLoS ONE* **13**, (2018).
88. Smith-Arica, J. R. & Bartlett, J. S. Gene therapy: Recombinant adeno-associated virus vectors. *Current Cardiology Reports* **3**, (2001).
89. Pacak, C. A. & Byrne, B. J. AAV vectors for cardiac gene transfer: Experimental tools and clinical opportunities. *Molecular Therapy* vol. 19 (2011).
90. Urabe, M. *et al.* Scalable Generation of High-Titer Recombinant Adeno-Associated Virus Type 5 in Insect Cells. *Journal of Virology* **80**, (2006).
91. MacLennan, D. H. & Kranias, E. G. Phospholamban: a crucial regulator of cardiac contractility. *Nature Reviews Molecular Cell Biology* **4**, 566–577 (2003).
92. Gomes, A. v, Potter, J. D. & Szczesna-Cordary, D. The role of troponins in muscle contraction. *IUBMB life* **54**, 323–33 (2002).
93. Verardi, R., Shi, L., Traaseth, N. J., Walsh, N. & Veglia, G. Structural topology of phospholamban pentamer in lipid bilayers by a hybrid solution and solid-state NMR method. *Proceedings of the National Academy of Sciences of the United States of America* **108**, (2011).
94. Fisher, Ml. E. *et al.* Dwarf open reading frame (DWORF) peptide is a direct activator of the sarcoplasmic reticulum calcium pump SERCA. *bioRxiv* **53**, (2020).
95. SIMMERMAN, H. K. B. & JONES, L. R. Phospholamban: Protein Structure, Mechanism of Action, and Role in Cardiac Function. *Physiological Reviews* **78**, 921–947 (1998).
96. Vostrikov, V. v, Soller, K. J., Ha, K. N., Gopinath, T. & Veglia, G. Effects of naturally occurring arginine 14 deletion on phospholamban conformational dynamics and membrane interactions. *Biochimica et biophysica acta* **1848**, 315–22 (2015).
97. Minamisawa, S. *et al.* Chronic phospholamban-sarcoplasmic reticulum calcium atpase interaction is the critical calcium cycling defect in dilated cardiomyopathy. *Cell* **99**, (1999).
98. Chu, G. *et al.* Phospholamban ablation and compensatory responses in the mammalian heart. *Annals of the New York Academy of Sciences* **853**, (1998).
99. Luo, W. *et al.* Targeted ablation of the phospholamban gene is associated with markedly enhanced myocardial contractility and loss of β-agonist stimulation. *Circulation Research* **75**, (1994).
100. Hoshijima, M. *et al.* Chronic suppression of heart-failure progression by a pseudophosphorylated mutant of phospholamban via in vivo cardiac rAAV gene delivery. *Nature Medicine* **8**, (2002).
101. Cure PhosphoLambaN induced cardiomyopathy (CURE-PLaN). https://www.cure-plan.online/ (2021).
102. Stichting Genetische Hartspierziekte. https://plnheart.org/ (2021).
103. Karakikes, I. *et al.* Correction of human phospholamban R14del mutation associated with cardiomyopathy using targeted nucleases and combination therapy. *Nature Communications* **6**, (2015).

104. Hajjar, R. J. & Hulot, J. S. Modeling CVD in human pluripotent cells by genome editing. *Journal of the American College of Cardiology* vol. 64 (2014).
105. Mearini, G. *et al.* Mybpc3 gene therapy for neonatal cardiomyopathy enables long-term disease prevention in mice. *Nature Communications* **5**, (2014).
106. Jiang, J., Wakimoto, H., Seidman, J. G. & Seidman, C. E. Allele-specific silencing of mutant Myh6 transcripts in mice suppresses hypertrophic cardiomyopathy. *Science* **342**, (2013).
107. Christidi, E., Huang, H. (Margaret) & Brunham, L. R. CRISPR/Cas9-mediated genome editing in human stem cell-derived cardiomyocytes: Applications for cardiovascular disease modelling and cardiotoxicity screening. *Drug Discovery Today: Technologies* vol. 28 (2018).
108. del Monte, F., Harding, S. E., Dec, G. W., Gwathmey, J. K. & Hajjar, R. J. Targeting phospholamban by gene transfer in human heart failure. *Circulation* **105**, (2002).
109. Watanabe, A. *et al.* Phospholamban ablation by RNA interference increases Ca2+uptake into rat cardiac myocyte sarcoplasmic reticulum. *Journal of Molecular and Cellular Cardiology* **37**, (2004).
110. Tiemann, K. & Rossi, J. J. RNAi-based therapeutics-current status, challenges and prospects. *EMBO Molecular Medicine* vol. 1 (2009).
111. Morihara, H. *et al.* Phospholamban Inhibition by a Single Dose of Locked Nucleic Acid Antisense Oligonucleotide Improves Cardiac Contractility in Pressure Overload-Induced Systolic Dysfunction in Mice. *Journal of Cardiovascular Pharmacology and Therapeutics* **22**, (2017).
112. Hinkel, R. *et al.* Inhibition of microRNA-92a protects against ischemia/reperfusion injury in a large-animal model. *Circulation* **128**, (2013).
113. Veedu, R. N. & Wengel, J. Locked nucleic acids: Promising nucleic acid analogs for therapeutic applications. *Chemistry and Biodiversity* vol. 7 (2010).
114. Bryant, D. H. *et al.* Deep diversification of an AAV capsid protein by machine learning. *Nature Biotechnology* (2021) doi:10.1038/s41587-020-00793-4.
115. Setten, R. L., Rossi, J. J. & Han, S. ping. The current state and future directions of RNAi-based therapeutics. *Nature Reviews Drug Discovery* vol. 18 (2019).
116. Sugo, T. *et al.* Development of antibody-siRNA conjugate targeted to cardiac and skeletal muscles. *Journal of Controlled Release* **237**, (2016).
117. Nelson, B. R. *et al.* A peptide encoded by a transcript annotated as long noncoding RNA enhances SERCA activity in muscle. *Science* **351**, 271–275 (2016).
118. Makarewich, C. A., Bezprozvannaya, S., Gibson, A. M., Bassel-Duby, R. & Olson, E. N. Gene therapy with the DWORF micropeptide attenuates cardiomyopathy in mice. *Circulation Research* (2020) doi:10.1161/CIRCRESAHA.120.317156.
119. Doevendans, P. A., Glijnis, P. C. & Kranias, E. G. Leducq Transatlantic Network of Excellence to Cure Phospholamban-Induced Cardiomyopathy (CURE-PLaN). *Circulation Research* vol. 125 (2019).
120. Stillitano, F. *et al.* Genomic correction of familial cardiomyopathy in human engineered cardiac tissues. *European Heart Journal* **37**, (2016).